In Vivo Characterisation of Human Calcaneal Soft Tissue

by

Alexandre Santana

This thesis is submitted in partial fulfillment of the requirements for the degree of MPhil in Bioengineering

Bioengineering Unit
University of Strathclyde
Glasgow, UK
2011

Copyright statement

Signed: Date:

Acknowledgments

To Vinícius.
To Ana and Bruno.

Without him I wouldn't have started.
Without them I wouldn't have finished.

Contents

List of Figures

List of Tables

List of Equations

Abstract

The calcaneal fat pad is a fibro-adipose tissue that is organized to bear stress and dissipate the shock associated with activities of everyday living. Research characterising the structural properties of the plantar fat pad *in vivo* is lacking, therefore this study aimed to evaluate the ability of Movement Analysis Systems (MAS) to measure the structural properties of the calcaneal fat pad in humans during a dynamic loading and unloading task.

A study to test the accuracy of the MAS to measure small deformations was executed, consisting of a comparison between the results obtained using this equipment to collect displacements and a force platform to gather load values with data acquired in similar conditions in reference equipment. Silicone rubber samples were submitted to the same loading and unloading procedure using both methods, and the vertical deformation recorded. The RMS of the differences between equipments can be considered a trend for the systematic error found on the MAS, corresponding to an underestimation of 0.3 mm.

Sequentially, sonographic evaluation of the heel pad thickness of 16 healthy adults was done. Hemispheric makers were attached to the heel of each subject at prescribed locations. A MAS using six cameras synchronised with a force platform was used to record 3-D displacements of the heel pad during loading and unloading exercises. The calcaneal fat pad deformed 8.0 mm vertically, 3.1 mm medio-laterally, and 2.6 mm posteriorly. The mean Compressibility Index was 0.50, and the mean stiffness for all subjects was 212 kN/m, however males shown a heel 47% stiffer than females. The energy dissipation ratio found for all participants was 22.3%.

The structural properties of the calcaneal fat pad can be estimated using 3-D MAS synchronised with a force platform. Preliminary findings suggest that males may have stiffer fat pads than females despite similar initial thickness.

1. Introduction

1.1. Background

The calcaneal fat pad is a highly specialized fibro-adipose tissue in humans that is organized to bear stress and dissipate the shock associated with activities of everyday living. However, it is unclear if conditions like plantar heel pain are influenced by a deficient shock absorbency caused by altered heel pad morphology. It is suggested by many investigators that changes in structure, observed by the unloaded thickness of the fat pad, and structural properties associated with elasticity, like the compressibility index (the ratio of unloaded to loaded heel pad thickness), are related with the onset of this syndrome (Prichasuk, 1994; Turgut et al., 1999; Kanatli et al., 2001, Rome et al., 2002; Wearing et al., 2009). Potential gender differences on these properties in healthy subjects, on the other hand, have been poorly investigated, although it is known that the heel pad thickness is lower in girls and adult females (Mikle et al., 2008) and lower elasticity has been suggested to predispose females to musculoskeletal injury (Ozdemir et al., 2004).

Heel pad has been reported to be thicker in men than in women when measured on both unloaded and loaded states using radiography (Prichasuk et al., 1994; Prichasuk, 1994; Turgut et al., 1999) or ultrasound methods (Uzel et al., 2006a), but no significant difference has been found on the compressibility index, generally taken as a measure of elasticity. These gender studies contribute to the understanding of static or quasi-static conditions, however they do not evaluate how the heel pad behaves dynamically, where viscous factors can affect time-dependent responses. Investigations on stiffness using ultrasound and indentation equipment have been conducted to characterize the heel pad under loading and unloading conditions. No agreement on the values is found in the literature with quoted values for healthy subjects, ranging from higher than those from individuals with plantar heel pain to lower values than them (Tsai et al., 1999; Rome et

al., 2001). These studies used peak loading values far less than those found in normal gait, and provide no report on the influence of gender.

1.2. Project aims

Although many works adopted dynamic methods to evaluate structural properties of the heel pad, varying from materials testing machines or pendulum tests on *in vitro* cadaveric heel samples (Bennett and Ker, 1990; Aerts et al., 1995; Aerts et al., 1996; Ker, 1996) or indentation on *in vivo* subjects (Hsu et al., 1998; Tsai et al., 1999), no study has yet explored the three-dimensional behaviour of the heel pad submitted to cyclic compression loading, and there is still a lack of knowledge whether these properties behave differently on males and females.

The aim of this investigation was to characterize the dynamical behaviour of the human calcaneal soft tissue under loading, and evaluate the influence of gender on the results. Deformation values on three-dimensions captured with a motion analysis system combined with loading and unloading data acquired on a force plate form the basis of the proposed method of determining stiffness of the tissues.

1.3. Project overview

This method will use hemispherical retro-reflective markers of 3 mm in diameter attached to the heel pad of healthy volunteers performing cycles of a pre-determined exercise to compress their foot against a force platform. A group of motion analysis cameras will capture the three-dimensional coordinates of the markers and the results, combined with force platform data, will be used to estimate structural properties of the calcaneal fat pad.

As a pilot investigation, an evaluation of the motion analysis system accuracy when capturing movement in the order of magnitude of the heel pad deformation reported in the literature using 3 mm markers was performed. A test using silicone tissue phantoms was conducted, the phantoms were vertically compressed using two methods, motion and force analysis and, as a reference method, a materials testing machine. A comparison between the compression results obtained with these different methods was used to evaluate the accuracy of the proposed motion analysis and force plate method. Subsequently the method was used to investigate the tissues properties of the heel pad in healthy male and female volunteers.

Therefore, this work starts on Chapter 2, with an overall literature review where theoretical aspects of the heel pad are discussed, with a description of the most common methods used to measure its structural properties. Thereafter, a critical reading of the most relevant reports on this theme is presented, focused on the properties analyzed in this project.

The description of the silicone tissue phantom test is made on Chapter 3, including an explanation of the equipment used and the test protocol conducted, followed by the data analysis, the results obtained, and a discussion on the accuracy of the motion analysis system.

The human test data is presented in Chapter 4, where both the system setup and procedure are explained, the results presented, and a discussion

comparing the findings with those already reported on the literature is given. The Chapter 5 gives the discussion and conclusions of this work.

2. Literature Review

This chapter describes the foot anatomy, giving special focus on the heel pad and its functional properties, both in normal conditions and in disease. A general description of the structure and structural properties, object of interests of this study, is given, and also the methods generally used to acquire these values. Finally, results obtained from several studies are shown, in order to provide data to compare with this investigation's findings.

2.1. Heel pad anatomy & function

The foot is composed of twenty-six bones connected by ligaments, with muscles and soft tissues surrounding them, and covered with skin. It can be divided into three segments, accordingly to position. The forefoot is located most anterior, and comprises the five metatarsal bones and the fourteen phalanges. Five bones make up the midfoot: three cuneiforms (medial, intermediate and lateral) plus the cuboid and the navicular. The most posterior segment is the rearfoot (or hindfoot), which consists of the calcaneus, the talus, and the surrounding soft tissues (Sammarco, 1988), as seen in Figure 2.1. Due to the objectives of this study, all the descriptions on this chapter will be related to the rearfoot.

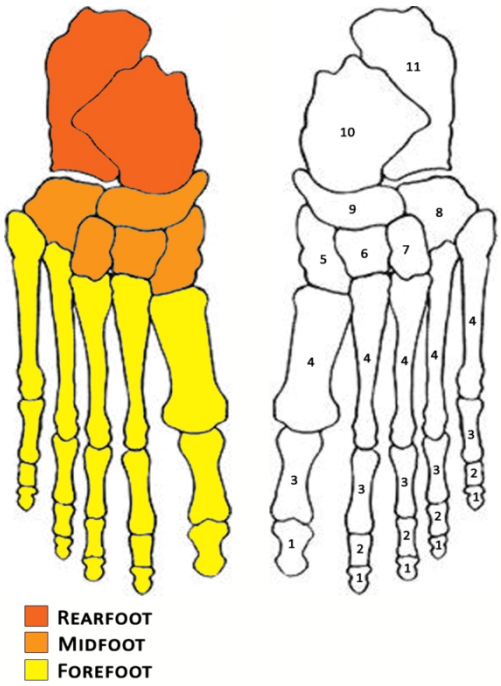

FIGURE 2.1 – Foot bones and segmentation. 1 = Distal phalanges; 2 = Middle phalanges; 3 = Proximal phalanges; 4 = Metatarsals; 5 = Medial cuneiform; 6 = Intermediate cuneiform; 7 = Lateral cuneiform; 8 = Cuboid; 9 = Navicular; 10 = Talus; 11 = Calcaneus.

The two bones of the rearfoot act as a structural pillar that supports the forces produced by the human weight either standing, walking, or running. Amongst the ankle or tarsal bones, which are the sum of the midfoot and rearfoot bones, the calcaneus and talus are the largest (Martini, 2006). The first of these bones to receive the weight is the talus, located proximally and articulated with the tibia through both the superior and medial surfaces of the process called trochlea. The force exerted on the ground, which goes proximal to distal, passes from this point to the calcaneus across the subtalar (or talocalcaneal) joint, on its posterior facets.

The tuber or calcaneal process is the most inferior and strongest portion of the calcaneus and the first to contact the ground when walking or running in normal conditions, this is guaranteed by the normal calcaneus when positioned with an anterior elevation of 15° from the horizontal plane at first contact (Dykyj, 1999). The tuber is anatomically described as having two distinct processes: medial and lateral, with the first from 15 mm to 20 mm in diameter and the second with 10 mm in diameter. Thus, on the coronal plane, the calcaneus is positioned more inferior medially than laterally.

These areas give attachments for the connective tissue that maintains the arch of the foot – the plantar deep fascia, or plantar aponeurosis -, and also for origins of some plantar muscles.

Mainly anchored to the plantar aponeurosis through collagenous junctions (Blechschmidt, 1982) and extending until the epidermis of the heel is the fat pad of the sole of the foot. On a general description, the heel pad is composed by adipose tissue constrained within walls made by a mesh of elastic and collagenous fibers. These closed chambers are called septum or septa (plural) and can also be anatomically related to any division between two tissues or cavities.

Septa

The main function of these several septa within the heel pad is to restrain movement of adipose tissue, therefore providing shock absorption in response to the forces created by ambulation. Consequently, to yield this feature, the fat tissue enclosed in the fiber container must work as an incompressible liquid when submitted to external loading. This means that the septa can change its shape when loaded, however its volume does not suffer any change.

Jahss et al. (1992b) injected India ink into cadaveric atrophic heel pads to evaluate the existence of breakdown on the chambers walls. They were unable to see any interseptal ink leakage, which suggests the adipose tissue does not flow across chambers even in diseased heel pads.

Elastin and Collagen

The septal wall is made of a mesh of collagen and elastic fibers has two distinct properties that help to resist tension without rupture: strength and flexibility. Collagen is the protein responsible for giving structure to connective tissue in the human body. It is resistant to ruptures and strong, and can be found in muscles, tendons, cartilages, bones, and also contributes as a support framework to cells in various tissues.

Elastin is the basic protein that makes up elastic fibers. As its name suggests, it has spring like properties that maintain its original length even after being submitted to stretching. Both fibers types, collagen and elastic, are organized as strands of a rope, according to Martini (2006). Therefore, the fibers are flexible when submitted to buckling or bending loads, however they are extremely difficult to pull apart in a longitudinal direction.

Thus, the septum can change its shape when loaded, recoiling without losing its contents, and returning to its original form after the load is removed. The elastic fibers act as the spring mechanism giving elasticity, and the collagen fiber being the structural component, inhibiting the chamber rupture.

The amount of elastic and collagen fibers on each layer of the cutaneous membrane that forms the fat pad and the chamber size are two factors that determine the mechanical properties of each layer. Figure 2.2 shows how the heel pad is histologically divided, starting from the outer skin layer, the epidermis, and extending to the plantar aponeurosis and calcaneous.

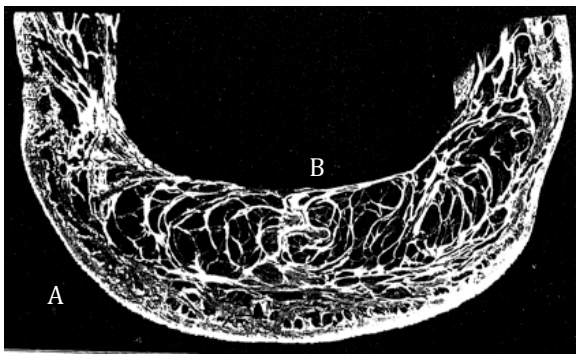

FIGURE 2.2 - Heel pad cutaneous membrane. (Blechschmidt, 1982). A = Outer skin; B = Plantar aponeurosis.

Microchambers and Macrochambers

From the external skin up to the calcaneous bone, the heel pad can be divided into several layers. A thick epidermis forms the heel skin, and this outer coat gives support to the attachment of the second layer, the papillary dermis, which has around 5% to 10% elastic tissue interlaced with collagen. The following layer, the reticular dermis, has more elastic characteristics due the presence of 40% to 50% of elastic fibers on its volume. Joining this first group is the superficial subcutaneous layer, with approximately the same amount of collagen and elastic fibers (Buschmann et al., 1995). All these three layers contain small adipose tissue chambers and can be named as superficial microchamber (Hsu et al., 2007).

A thick horizontal septa separates the microchamber layer to the thickest macrochamber layer. The septa on the deep subcutaneous layer are more elastic (50% to 60% of elastic fibers), significantly larger than those of the microchamber, and are oriented vertically (Buschmann et al., 1995). The deeper septa are attached to the plantar aponeurosis by collagen fibers, and the aponeurosis, in its turn, is eventually connected to the periosteum of the calcaneus. Some elastic fibers can also be seen attached to the aponeusoris.

The distinction of two layers on the fat pad according to chamber size and elastic tissue composition can lead to different mechanical properties for each. The large vascular network in the microchamber also contributes to

increase the amount of elastin (present in blood vessels) in this layer (Jahss et al., 1992a). This was supported by Hsu et al. (2007), who found distinctive values to stiffness on the microchamber and the macrochamber. The present study will not take into account two different types of adipose tissue, all the analysis will occur on the soft tissue as a unique entity, starting from the epidermis and going to the plantar aponeurosis.

Septa shapes

Septa structure varies accordingly to its position, from U-shaped to comma shaped, however they are mostly distributed vertically because of their compressive resistance function. Several factors can affect their mechanical properties, such as volume, location, and constitution of fat pad, and the biomechanical behavior is similar to globular or cylindrical bodies under vertical loading (Jahss et al., 1992a).

Tension on shapes similar to that found within septa walls is proportional to their radius and the pressure applied, accordingly to Young-Laplace's equations (Pellicer et al., 2000). On the septa case, the vertical pressure acts on a very small area, which leads to a curvature on the lateral surface, inwards or outwards. Septum size also has impact on the deformation behavior, and the way they are grouped contributes to increase the amount of elastic and collagen walls present, therefore the septum will be stiffer. The wall thickness is another variable that influences the deformation, so if the structure is thicker, it means the septum is more resistant to deformations. Therefore, depending on the septum size, geometry and structure, it can deform differently, following the patterns of Figure 2.3 (Jahss et al., 1992a).

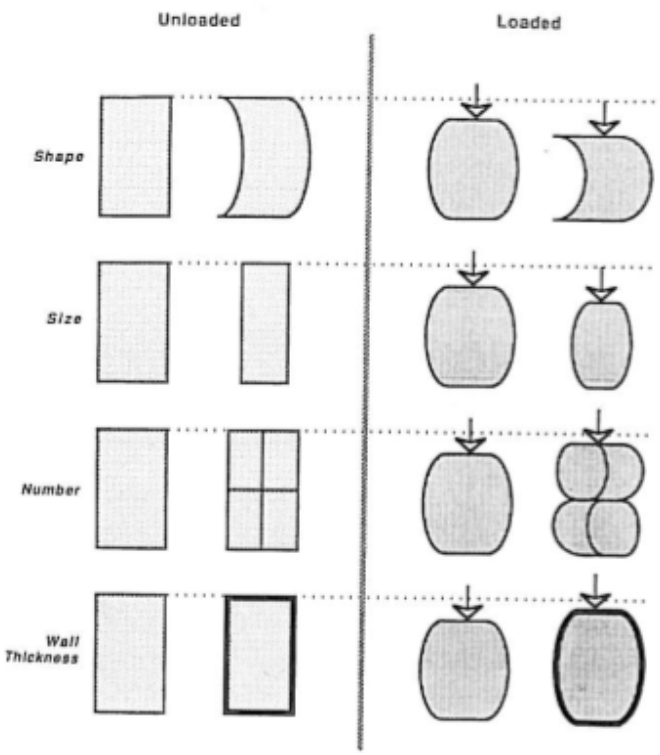

FIGURE 2.3 – Septa deformation patterns and factors. (Jahss et al., 1992a).

All these considerations regarding the normal anatomy of the heel and its fat pad can also be applied to the heel pad in disease, in addition to structural factors that can lead to pain or discomfort, such as fat composition and breakdown of the septa. The next session will detail these conditions and how the heel pad mechanical properties can be affected.

2.2. Heel pad in disease

Since their early ages, humans compress their heel pads numerous times each day, standing, walking or running. These mechanical loading and unloading cycles have been hypothesized to lead to a series of structural problems that may eventually lead to pain, however systemic diseases can also be the primary reason for such conditions.

Chronic Plantar Heel Pain (CPHP) is amongst the major common foot disorders and is typically associated with pain in the medial aspect of the heel, particularly during the morning or when under loading conditions, such as at the first steps of the day. It is not directly related to gender, however it is most seen with over 40 years people. Due to the poorly understood aetiology of CPHP, this term has become a general name of a series of distinct diseases such as plantar fasciitis, subcalcaneal bursitis and subcalcaneal pain, neuritis, spur, stone bruise, calcaneal periostitis, calcaneodynia and achillodynia (Irving et al., 2006).

Systemic diseases can also lead to heel pain, although foot deformities are another consequence of them. Amongst these diseases, one can point out rheumatoid arthritis, diabetes mellitus, and osteoporosis, however, accordingly to review of the topic by Lichniak (1990), other conditions can also occur including crystal deposition arthropathies, diffuse idiopathic skeletal hyperostosis, hypertrophic osteoarthropathy, Paget's disease, hyperlipidemia, sarcoidosis, sickle cell anemia, and acromegaly.

Either generic CPHP or systemic diseases show pain as the ultimate outcome, and although the aetiology is not yet conclusive, the heel pad structure generally appears modified in these conditions. Comparable to normal fat pads, an atrophic heel is defined by Jahss as “thinner, more closed attached to the calcaneus, and less dense and, upon pressure, the underlying bone could be palpated” (Jahss et al., 1992a). These characteristics might be consequence of an altered composition of the adipose tissue and/or rupture of the fibrous septa wall (Buschmann et al., 1995).

Therefore, changes on structure and mechanical properties of the heel tissue are indicators of disease, and can be used as a clinical diagnostic tool. Consequently, an understanding of how both structure and mechanical properties behave on healthy and abnormal heels is essential.

2.2.1. Structure

As described earlier, the heel soft tissue is a series of closed chambers composed mainly by two entities: an inner layer of adipose tissue covered by an external wall made up of bundles of collagen and elastic fibers. Therefore, any disarrangement of these elements can alter the mechanical properties of the heel pad, and many authors suggested that a loss of elasticity might be one of the heel pain causes (Prishasuk, 1994; Tsai et al., 1999; Turgut et al., 1999).

Molecules and suspended materials in a liquid can interact and promote resistance to flow, this is called viscosity (Martini, 2006). The adipose tissue enclosed within the septa is composed of saturated and unsaturated fatty acids, and different ratio of these two components can modify the viscosity of the fat pad. It was described by Buschmann et al. (1993) that in normal heel pads, the concentration of unsaturated fatty acids is high and the saturated fatty acids low, when compared with abdominal adipose tissue. This may promote a reduction in viscosity, potentially contributing to changes in shock absorbency properties.

The intricate septa architecture is much more susceptible to deformities and these changes are largely described in the literature. A mesh of collagen and elastic fibers surrounds the adipose tissue and is reinforced by other transverse and diagonal fibers (Jahss et al., 1992a). Traumatic, degenerative or aging processes can originate the rupture of these fibers, probably affecting the chambers internal support (Hsu et al., 1998; Jahss et al., 1992a; Jahss et al., 1992b; Turgut et al., 1999; Buschmann et al., 1995).

The breakdown of this network can lead to a thinner heel pad under loading because it might permit an increase in bulging on compression. The elastic fibers, which are initially responsible for the spring like properties, appear in a greater number, but thicker and generally fragmented. This can contribute to loss of the rebound characteristic, consequently decreasing the resilience. Connected to this fact, the inelastic collagen fibers also show

altered pattern, aggregated in large bundles (Jahss et al., 1992b). Figures 2.4a and 2.4b show normal and abnormal structures of fat pads, the increase in fibers thickness can be seen in Figure 2.4b.

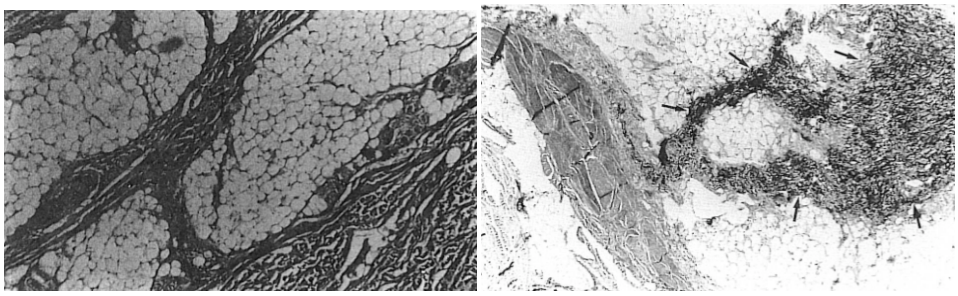

(a) (b)

FIGURE 2.4 – (a) Calcaneal fat pad in a normal young foot. (b) Senescent dysvascular foot (Jahss et al., 1992b).

Although the fibers have shown altered architecture, with ruptured elastic bundles on the septa, it is important to mention that no fluid or internal chamber content flow was reported between septa. This reveals that the integrity of the structure is still maintained, even in the presence of degenerative processes.

2.2.2. Properties

Although interest in the aetiology of the heel pain has grown lately, there is neither comprehensive nor conclusive literature regarding the structural properties of the heel pad in disease (Wearing et al., 2009). It is still not clear how four key heel pad properties behave under loading, due to conflicting evidence or limited techniques. Thickness, elasticity, stiffness and energy dissipation ratio are the properties often used to characterize the fat pad, and there are different methods to measure them, as will be seen in details in section 2.4.

The **Thickness**, a structural characteristic of the heel pad, is generally measured from the inferior aspect of the medial tuber until the superficial skin. Ultrasound and X-ray are common methods to observe it, both on loaded or unloaded states. When comparing diseased to asymptomatic heels, most studies show no difference in thickness (Kanatli et al., 2001; Tsai et al., 1999; Turgut et al., 1999; Wearing et al., 2009). However, a correlation between age and an increased thickness was observed (Prichasuk, 1994; Hsu et al., 1998).

To evaluate the ability to absorb shock, a diagnostic method called **Compressibility Index (CI)** was created as a measurement of elasticity (Jørgensen, 1985). This index is the ratio of unloaded to loaded heel pad, therefore the greater the value, the less elastic the fat pad is. For instance, plantar heel pain is suggested to be associated with the loss of that elasticity because the fat pad can act as a damper to the vibrations generated by the dynamic forces of gait (Tsai et al., 1999). The CI values for patients with this condition are higher than those found in healthy subjects (Prichasuk, 1994; Wearing et al., 2009).

However, when comparing painless and painful heels, the CI values found in the literature do not agree. Some studies reported no correlation between flexibility and heel pain (Kanatli et al., 2001; Tsai et al., 1999; Turgut et al., 1999), although higher CI values were found on symptomatic heels

(Prichasuk, 1994). The lack of a controlled and standard loading method to measure the fat pad thickness has perhaps influenced these findings. Moreover, the quasistatic technique adopted largely in these studies does not simulate gait conditions, which might lead to the discrepancies in the results (Wearing et al., 2009).

Another property commonly analyzed is the resistance to deformation by an applied force, called **Stiffness**. This property takes into account the material behavior over time, which helps the characterisation of viscous factors associated with soft tissues. The non-linear loading response from those tissues is generally correlated to an increase on the stiffness during time, with the opposite occurring during unloading. Thus, soft tissues viscoelastic characterisation can be derived from time-dependant observation (Hsu et al., 2002). A few studies have tried to report stiffness using these curves, but the methods applied do not replicate gait-loading situations.

Viscoelastic materials also have another descriptive characteristic, the existence of hysteresis. This non-linear feature is clearly seen on loading-unloading curves, and is represented by the area between the two arms of the curve. Unlike elastic elements, human soft tissue absorbs energy associated with deformation when loaded and releases it during the unloading phase of the gait cycle, always dissipating a percentage as heat (Hsu et al., 1998). This absorbed energy is recognized as the **Energy Dissipation Ratio (EDR)**, and is associated with the shock absorbency of the fat pad. It is defined as follows:

$$\%\ \text{Energy absorbed (EDR)} = \frac{(\text{Energy input} - \text{Energy returned})}{\text{Energy input}} \times 100\%$$

Equation 2.1 – Energy Dissipation Ratio (EDR).

Values of EDR vary greatly, accordingly to the method adopted to apply the load-unload regimen. Therefore, no conclusive data were found in the literature analyzing symptomatic and non-symptomatic heels. Diabetic patients show high EDR due to an increased unloading curve (Hsu et al.,

2002), however the same behavior was not observed on plantar heel pain subjects compared to controls (Wearing et al., 2009). Conflicting results were found when comparing elderly people with young, showing both high and low EDR values (Hsu et al., 1998; Kinoshita et al., 1996). The different techniques used to apply the deformation on the heel might have influenced these contradictory findings.

In the next section, a deeper analysis will take place on the various methods used to evaluate the heel pad structure and the structural properties. Sequentially, results for these properties reported in several studies will be presented.

2.3. Methods for evaluating structure and structural properties

Several methods have been used to evaluate the heel pad structure and estimate its structural properties. These properties are influenced by the composition of the hell pad, i.e. the adipose-chambered tissue and the elastin/collagen surrounding wall. Thickness, deformation, compressibility index, stiffness and energy dissipation ratio are amongst them and have been widely described in the literature. On the other hand, mechanical properties, which take the structure into account, are less frequently reported and involve stress, strain, and modulus (Ledoux and Blevins, 2007). Because the present study is based on deformation and force data, as will be seen on chapters 3 and 4, only structure and structural properties studies will be analyzed in this section.

The methods for evaluating structure are often qualitative and can be as simple as a clinical palpation of the calcaneal area, on the other hand they can use precise imaging devices such as magnetic resonance image (MRI) machines. In between are X-rays, ultrasonography (US), impact tests, indentation, computational tomography (CT), and motion analysis. This section will focus on the description of these methods, while section 2.4. presents the values of the structural properties obtained with these various techniques.

Qualitative analysis

Although palpation and physical examination are widely used tools in foot and ankle clinical practice, stiffness and tenderness of the heel pad can be described only subjectively (Rome and Webb, 2000; Rome et al, 2001). For that reason, even with experienced investigators the findings may vary, which justify the lack of scientific literature on this method.

2.3.1. Radiographic/Fluoroscopic studies

The use of radiographs or fluoroscopic images to measure angles and distances is common in clinical practice, with results validated in the literature (Saltzman et al., 1994). In the case of the heel pad, lateral images are taken to evaluate the thickness of this adipose tissue, in both loaded and unloaded conditions. Based on these images, the Compressibility Index (CI) was created to evaluate the shock absorptive ability of the heel pad (Jørgensen, 1985), and this is one of the most frequent diagnostic tools to evaluate heel atrophy. Deformation values are easily measured from loaded and unloaded X-rays.

Radiography

Although the technique has been used for many years, there are two effects that raise discussion. An inherent problem of X-rays is the magnification effect, in which real distances and angles appear augmented on the radiographic image. Some procedures can be applied to correct this issue, reducing the errors (Wearing et al., 2009), but this can be time consuming.

The second issue is related to the exposure to radiation. Although this point is a matter of discussion, studies have stated the exposure is less than maximum levels, for example: 0.02 times the allowed annual dose by Belgian law (de Clercq et al., 1994) or 35 times less than annual exposure to other sources like sun or television beams (Wrbaskić and Dowling, 2007).

Fluoroscopy

Unlike radiographs, fluoroscopy or cineradiography are methods that show dynamic states. Although they use the same basic principle, which is the emission of radiation to see bony structures and also soft tissues, they can collect a sequence of images that help in evaluating movement. The shortcoming is an increase of exposition of the subject to radiation. However, a few studies have used these methods to gather true gait data, which improves the analysis from more than two singular loaded or unloaded pictures to a comprehensive gait cycle (de Clercq et al., 1994; Gefen et al., 2001; Wrbaskić and Dowling, 2007). The structural properties of the heel pad can be represented by deformation-time curves, and when force measurements are included using a force plate, can lead to dynamic force-deformation curves. Estimation of the energy dissipation ratio (EDR) can also be undertaken with these methods (Wearing et al., 2009). However, this study pointed out the clear restriction of the method to two-dimensional analysis on what is naturally a three-dimensional body.

These two imaging methods allow the determination of thickness, a basic heel pad structure, and a structural property, the Compressibility Index (CI). Fluoroscopy also allows the characterisation of time-dependent properties if the loading regimen is also known, like the Energy Dissipation Ratio (EDR), stiffness-time curves, and force-deformation curves can be developed.

Thickness

Thickness measurements are taken from the skin edge to the lowest part of the plantar tuberosity of the calcaneus, on both loaded and unloaded

settings (Prichasuk et al., 1994; Prichasuk, 1994; Cavanagh et al., 1997; Turgut et al., 1999; Kanatli et al., 2001), accordingly to the Figure 2.5.

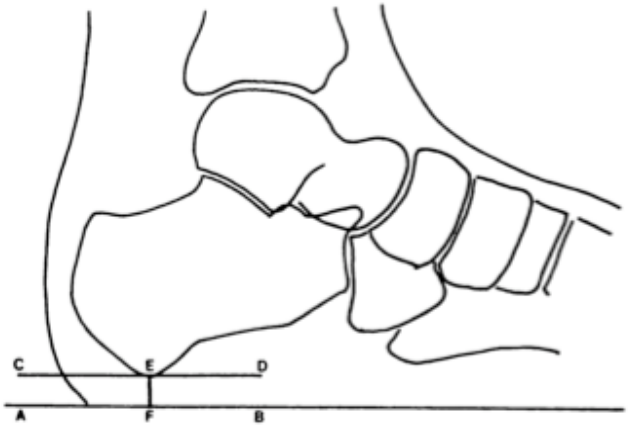

FIGURE 2.5 - Heel pad measured at shortest distance between calcaneus and plantar surface of the skin (EF). AB = the skin line; CD = the longest part of the plantar tuberosity of the calcaneus. (Turgut et al., 1999).

Compressibility Index

The CI was created as a diagnostic test to evaluate the heel shock absorbing ability based on measurements of the unloaded and loaded heel pad (Jørgensen, 1985). As a relatively cheap and highly precise tool, it helps to diagnose a lack of shock absorbing capability on fat pads from two single radiographs images. The images are taken from the sagittal plane, without any load and under body weight load. The thickness of the heel pad is measured from the distance between the most distal aspect of the calcaneus tuberosity and the plantar surface of the skin, as shown on the Figure 2.5. The CI is as follows:

$$\text{Compressibility Index (CI)} = \frac{\text{loaded thickness}}{\text{unloaded thickness}}$$

Equation 2.2 – Compressibility Index (CI).

Thus, as the index approaches 1, it means that both loaded and unloaded thicknesses have almost the same value, therefore the shock absorption capability of the heel pad tends to be null.

2.3.2. Ultrasonography

Ultrasonographic examinations have been used to diagnose various diseases that affect the foot, such as plantar fasciitis, rheumatoid arthritis, diabetes and calcaneal fractures (Alvarez-Nemegyei and Canoso, 2006). Ultrasounds portability and relatively low cost compared to other imaging diagnostic tools make it a regular choice for clinicians to evaluate the heel pad structure. Another factor that contributes to this preference is that the technique neither uses radiation nor has the magnification effects of X-rays.

The most used ultrasound technique to measure heel pad structure is real-time B-mode imaging. The sound waves emitted by the probe reach a hard structure, which reflects the pulse back to the origin. The system uses the time taken for the sound to travel backwards and forwards to calculate the distance between the object and the probe based on velocity of sound in that media. This is 1.540 m/s for soft tissues. Different softer structures in-between the surface and bone can also be mapped in this way, and a two-dimensional image is created. For the calcaneal fat pad, the clinical benefit of ultrasound is on the determination of its thickness. Unloaded and loaded conditions can be evaluated based on different methods.

In all studies using ultrasound to measure heel pad thickness the sound wave emitted must reach the measured tissue without any loss to ensure that the probe and the plantar skin must be kept in contact. Normally a soluble acoustic gel is used as a coupling agent to reduce the air bubbles that could reflect or attenuate the ultrasound signal (Cavanagh, 1999).

Unloaded thickness is generally measured with the transducer, or probe, located in the middle of the plantar surface of the heel fat pad (Challis et al., 2008). The subject can be positioned either sitting or prone, with the foot placed at an angle of 90 degrees. The heel thickness is measured as the distance between the distal calcaneum and the transducer (Hsu et al., 1998), as seen in Figure 2.6a. Hand held probes gather the images, which can be post-processed or analyzed in real-time.

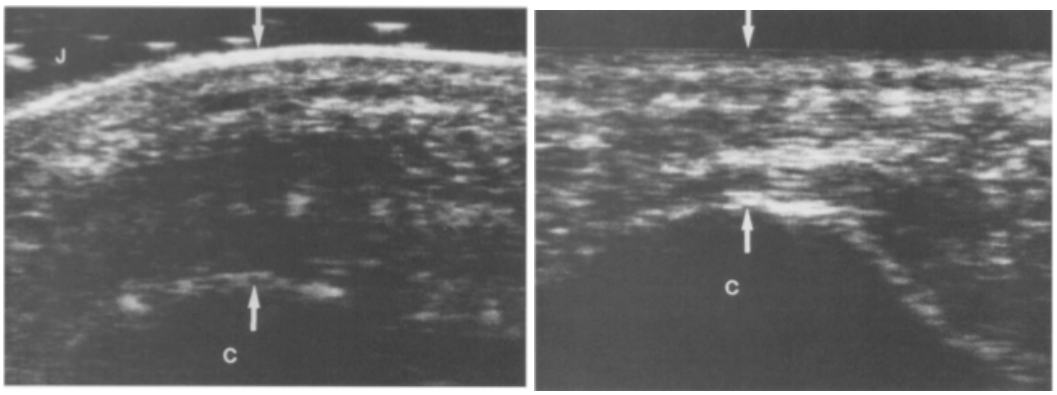

(a) (b)

FIGURE 2.6 – (a) Ultrasonography of the heel pad unloaded. A layer of soluble gel (J) was applied between the transducer and the plantar skin. The thickness is measured between the two arrows. C, calcaneus. (b) Ultrasonography of the heel pad loaded. The thickness is measured between the two arrows. C, calcaneus. (Hsu et al., 1998)

However ultrasound measures have an important limitation, namely the lack of repeatability on the probe position, caused by the fact that the images are captured in direction of the transducer and also require contact. In order to reduce this source of error, some authors used special devices to guarantee accurate placement of the foot and transducer. These devices can also be used to measure loaded conditions (Figure 2.6b), with a fixed probe and the heel being pressed against it using the body weight of the subject. Figures 2.7a and 2.7b show these two methods (Rome et al., 1998a; Cavanagh, 1999; Tsai et al., 1999; Rome et al., 2002).

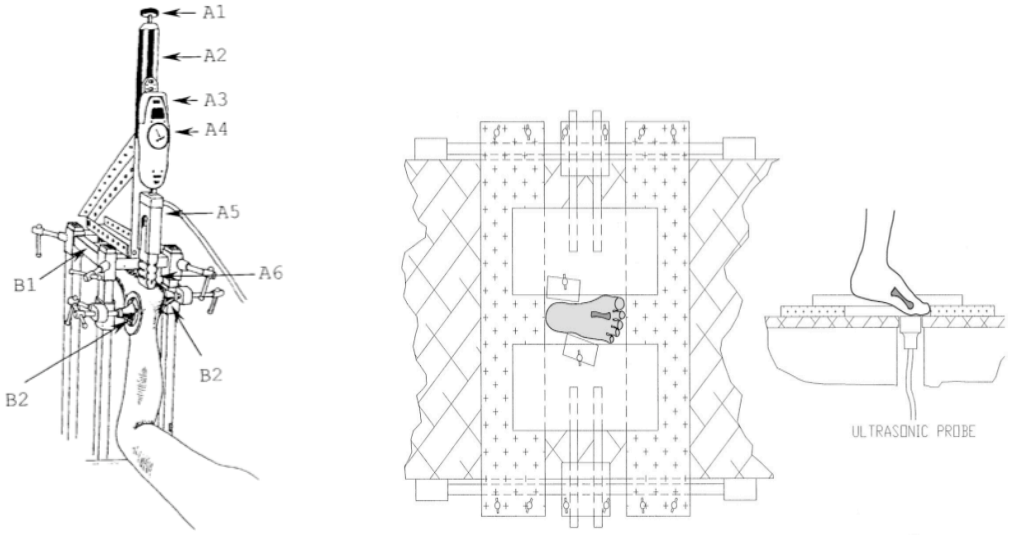

(a) (b)

FIGURE 2.7 – (a) Compression relaxation device used to measure heel pad thickness. A6 represents the moving ultrasound probe. (Tsai et al., 1999). (b) Fixed ultrasound device used to measure loaded thickness of the heel pad. (Cavanagh, 1999).

2.3.3. MRI & CT

Two other imaging techniques have been used to analyze heel tissue internal structure and estimate its properties, Magnetic Resonance Imaging (MRI) and Computed Tomography (CT). These are not common tools to this objective due to their cost. However, some studies have used them to obtain three-dimensional (3D) data from the fat pad.

MRI is a non-invasive exam where a machine emits electromagnetic waves to stimulate the body's atom nuclei, forcing them to a different position. These nuclei, when they return to the original position, generate an electromagnetic pulse, which is collected and processed by the machine. As the human body is formed mainly by water, the hydrogen atoms are used to this purpose and the amount of these atoms present in each tissue determines how it will be shown on the image. Dark areas represent low amount of hydrogen atoms, whereas brighter ones indicate tissues that contain a lot of water. The machines have a large magnet and the person being examined must be positioned lying inside it, which currently prevents standing examinations.

Being a non-invasive procedure, MRI does not expose subjects to an unhealthy agent. However, the use of a powerful magnetic field limits some testing protocols, as any metallic object cannot be used near the machine. Therefore, testing the compression of soft tissues like the heel pad with the subject being in a horizontal position, with a force being applied by an external ferrous metal apparatus, is not possible.

Computed Tomography does not provide the same image quality as MRI, but also has the ability to reconstruct body images in 3D. CT is a specialised type of X-ray, where a series of bi-dimensional radiographic images are taken from different angles, and an integrated computer can reconstruct the various body tissues according to the density of each.

The method can provide structural information from the heel pad tissue, but dynamic or quasistatic measurements are restricted. As on the MRI, the subject generally has to be in a horizontal position during the exam, which limits compression studies. Moreover, being an X-ray based technique and collecting a large amount of data in order to reconstruct 3D images, far more radiation is emitted than a standard X-ray.

Although these two methods can provide high quality images from the heel tissue, their restrictions to gather experimental data to analyze quasistatic or dynamic conditions led to just a few studies using them. Ordinary X-rays or ultrasound exams are cheaper than MRI or CT, adding another factor to the limitation. However, data from studies using these techniques can be used to create Finite Element Models (FEM) of the heel pad (Spears et al., 2005; Spears et al., 2007).

2.3.4. Impact tests

Pendulum and impact tests have been used mostly to gather mechanical properties of *in vitro* tissues. However, a few experiments have tried to estimate the behavior of heel pads in subjects using this method. Safeguarding of the subjects tested is a common issue. This method can be considered hazardous, since it is based on an impact principle, where a swinging mass of known value is thrown against the measured surface. This mass has an accelerometer attached to one of its edges, which captures the impact deceleration signal. The compression of the tissue being tested can be estimated by a double integration of this signal, providing time-dependant properties such as load-deformation cycles. Figure 2.8 shows a schematic model of the method, with a cadaveric foot.

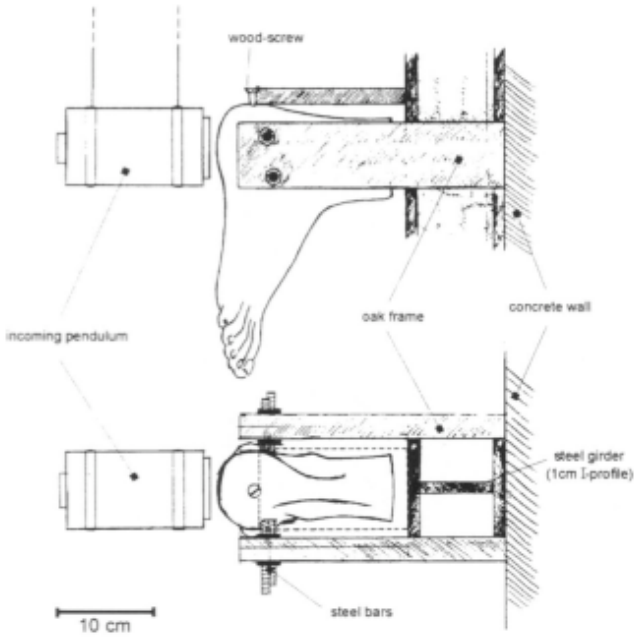

FIGURE 2.8 – Lateral and top views of a pendulum testing device used on *in vitro* tests. (Aerts et al., 1996).

Different configurations can be used to evaluate *in vivo* tissues, maintaining the same impact principle. Aerts and de Clercq (1993) carried

out a series of impact tests on a group of shod subjects in an attempt to evaluate the compressive behavior of the heel pad when fitted with shoes of varying midsole hardness, and the system set up for the experiment is showed in Figure 2.9a, where a known mass supported by cables is impacted into the shoe sole. A different set up was used by Kinoshita et al. (1996) to measure heel pad deformation on two groups of elderly adults and compare them with young adults, as seen in Figure 2.9b.

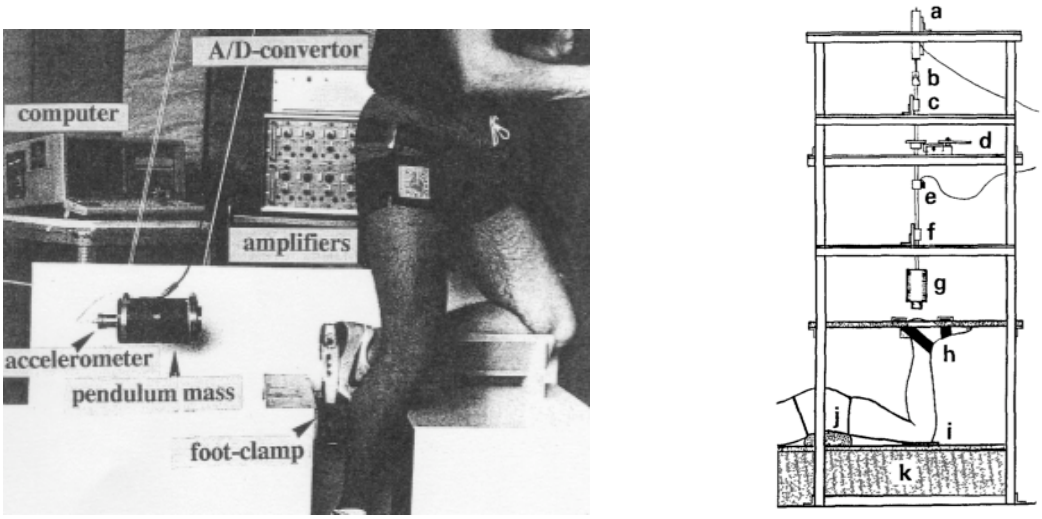

(a) (b)

FIGURE 2.9 – (a) Set up for the pendulum experiment. (Aerts and de Clercq, 1993). (b) Set up for the impact experiment (G) is the impact mass. (Kinoshita et al., 1996).

Some factors can affect the results obtained with these devices. The pendulum mass and the height on which the pendulum is thrown directly influence the compression force exerted on the foot, therefore, the amount of deformation depends on these variables (Aerts and de Clercq, 1993). Another limitation is that just a single impact is acquired, preventing the measurement of cyclic deformations.

2.3.5. Materials Testing Machine

Several structural studies on *in vitro* heel pads used compression testing machines (Bennett and Ker, 1990; Aerts et al., 1995; Aerts et al., 1996) to obtain displacement data, however, mechanical properties such as modulus can also be calculated using these devices (Ledoux and Blevins, 2007). Materials testing machine consist basically of a monitored load cell connected to a flat plate and another plate attached to a linear actuator. The relative displacement of these plates can be altered under a controlled rate, and the force exerted on the material being compressed or tensioned can also be measured. The servo-hydraulic Instron® machine is the most common device for this purpose. Figure 2.10 shows the main components of a compression materials testing machine.

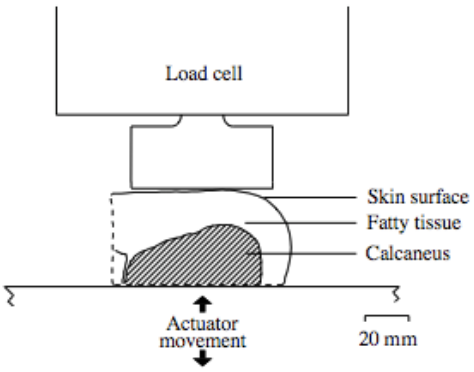

FIGURE 2.10 – Schematic model of a materials testing machine (MTM) with a cadaveric rearfoot being tested. (Ker, 1996).

Although these machines provide a large extent of control over the test protocols, like the force rate applied or the displacement required, the main restriction of this device is that it is limited to test materials samples, not *in vivo* human heel soft tissues. A discussion on the use of *in vitro* specimens to evaluate the structural and mechanical properties of the heel pad will take place in section 2.4.1.

2.3.6. Indentation

Indentation systems are usually used in conjunction with ultrasound equipment to help on the estimation of the mechanical properties of the heel pad (Ling et al., 2007). They have also been used without imaging techniques (Rome et al., 2001), or associated with MRI (Magnetic Resonance Imaging) or CT (Computed Tomography) on other soft tissue studies (Tran et al., 2007). While the ultrasound measures the thickness, the role of the indenter is to apply a controlled force to the system, thus load and displacement data can be collected, allowing the estimation of other structural properties, such as stiffness and energy dissipation ratio (Erdermir et al., 2006; Ling et al., 2007). Its portable characteristics help handling the device, however the loads applied are generally low when compared to body weight. To avoid this limitation, some authors used indentation systems as a starting point to feed Finite Element Models (FEM). Figure 2.11a shows a hand held indentation device and Figure 2.11b illustrates an indentation platform.

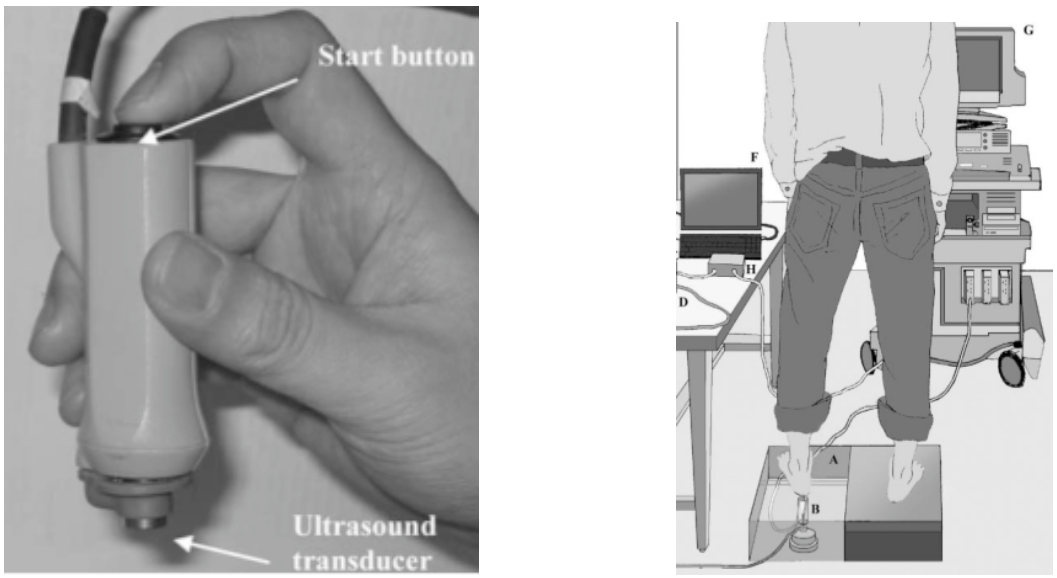

(a) (b)

FIGURE 2.11 – (a) Hand held indentation system with an ultrasound probe. (Ling et al., 2007). (b) Subject on a platform (A) composed by a couple of an ultrasound transducer and a load cell (B). (Hsu et al., 2007).

Indentation devices can also be mounted to obtain load-displacements curves without the use of an ultrasound machine. Rome et al. (2001) developed a portable instrumented device, consisting of a moving metal probe connected to a load cell, as illustrated in Figure 2.12. This device can be positioned on a platform where subjects stood, and a Linear Voltage Differential Transformer (LVDT) captures displacements, while force gauges (a group of strain gauges force transducers) on the moving shaft collect load values.

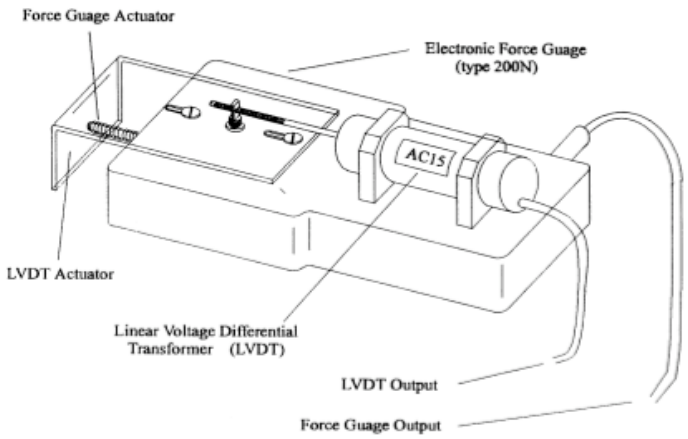

FIGURE 2.12 – Device used to measure loads and displacements on heel pads. (Rome and Webb, 2000).

Due to inclusion of the measurement of the force applied to the heel pad, indentation systems provide different information compared to other methods. However, generally these portable systems cannot apply high loads, which restrict comparisons of results obtained with different methods that use the body weight as the maximum load.

2.3.7. Motion Analysis

Movement analysis systems have been used clinically to various objectives: e.g. differentiate pathological from normal movements, evaluate the efficacy of treatments, or helping on the adjustment of walking aid devices such as orthosis and prosthesis. These systems collect quantitative data that describe how the subject moves, i.e. how his or her muscle-skeletal system acts to execute a specific task (Cappozzo et al., 2005). Several parts can be used in this analysis, some of them based on images of the body moving and others collecting external forces.

Photogrammetric systems are the basis of modern movement analysis (Wong et al., 2007). Using the same key principles of video recording, they capture images on two or three dimensions, using either reflective markers or light-emitting components attached to body landmarks. Special cameras obtain these markers or lights position and a computational system reconstructs them into spatial coordinates, allowing recognition of joint and body segments, and measurement of displacements, velocities, and accelerations.

Forces and moments applied on a flat instrumented surface can be measured by special dynamometers made up of a set of load cells, also known as a force platform. The load cells are often strain gauges embedded on a rigid surface that can collect force and moment data in three orthogonal axes in the space. For movement analysis purposes, this information is generally an external load applied by the subject being measured, for instance the ground reaction force on gait analysis. The reaction force on the body is then used to calculate internal loads, moments, work, and power. Figure 2.13 shows an example of a gait laboratory setup, where a subject walks along a walkway with a set of reflective markers attached on his body while a group of cameras capture the markers position and the force platforms measure the ground reaction force.

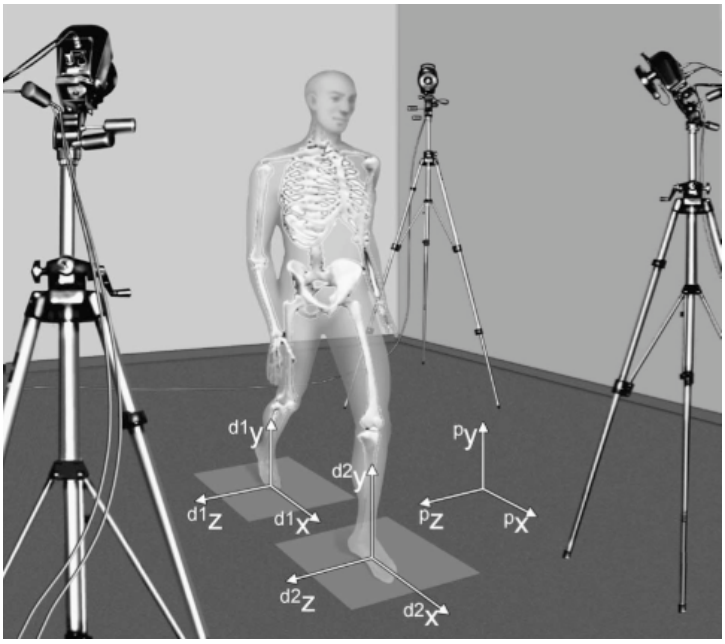

FIGURE 2.13 – Movement analysis laboratory setup. Stereophotogrammetric (p) and force platform (d) system axes are shown. (Cappozzo et al., 2005).

Used in conjunction, the camera system and force platform provide displacement and force data that can be used to determine the structural properties of the heel pad. However, just a few studies have applied this technique, moreover, they have used it as a complementary tool. Cavanagh (1999) used a VHS video camera in conjunction with ultrasound equipment to determine the heel pad thickness as a function of time when compressed. More recently, Chi and Schmitt (2005) employed a force platform and high-speed video cameras to gather force and deformation data of different walking patterns to estimate the energy absorbed by the heel pad during the impact phase. However, no study was found in which a movement analysis system had been used to measure the three-dimensional properties of the heel pad.

Three-dimensional analysis has been used largely in clinical and experimental gait analysis, with biomechanical reconstructive whole body models validated in the literature (McGinley et al., 2009; Yavuzer et al., 2008; Kadaba et al., 1990). Small deformations of the heel pad in 3D have not been assessed in such a methodological way, and hence this is one of the objectives of the present study.

2.4. Structure and structural properties of the heel pad

Stiffness, energy dissipation ratio (EDR), and the compressibility index are common heel pad structural properties described on the literature. The structure of the heel pad is also well described by studies investigating its thickness. Accordingly to the type of tissue studied (*in vitro* or *in vivo*) and the method used, the values can differ drastically, which prevents the determination of a unique set of these properties. Recently, methods using Finite Element Models (FEM) have tried to determine the relationship between these structural properties and derive constitutive equations to characterise the mechanical response of the heel pad to external loading (Miller-Young et al., 2002; Spears et al., 2005; Erdermir et al., 2006). However these methods will not be analyzed in the present study. The next sections show the most relevant investigations on the structure and the structural properties of the heel pad in both *in vitro* and *in vivo* specimens.

2.4.1. *In vitro*

During the 1990's an increase interest in the properties of the human calcaneal fat pad using human cadaveric materials arose. Amputated feet were used mainly because they provided a simplified way to be tested under controlled circumstances. A small sample could be placed both on a materials testing machine or submitted to a pendulum test, and structural properties measured, such as displacements under managed loading, allowing the depiction of stiffness and energy dissipation ratio (Bennett and Ker, 1990; Aerts et al., 1995; Aerts et al., 1996; Ker, 1996). More recently, fat tissue samples of the heel pad have been tested on materials testing machines to help calculating the constitutive equations of the material using Finite Element Models (Miller-Young et al., 2002; Spears and Miller-Young, 2006) or estimating materials properties like stress, strain and modulus (Ledoux et al., 2004; Ledoux and Blevins, 2007).

The importance of these studies is that they can provide the basis for comparisons with *in vivo* tests, as long as they were performed using a method that produces external disturbances compatible with *in vivo* methods, and also that the specimen tested represents the reactions of the living human body. Therefore, the first question is regarding the accuracy of the methods, and the second is about the type of sample being tested.

Trying to obtain answers to these questions Bennet and Ker (1990) obtained stiffness and EDR values from 11 amputated feet submitted to cyclic loading and unloading regimen using a materials testing machine. They found results quite different from those reported by pendulum tests done *in vivo* by that time. The EDR *in vitro* was described as being a third of that found on pendulum tests, and the authors justified this discrepancy stating that the pendulum exam takes into account the entire leg as an absorption system, which is impossible to do when testing *in vitro* small samples on materials testing machines.

Aerts et al. reported two studies (Aerts et al., 1995; Aerts et al., 1996) in which their group of researchers performed pendulum and materials testing machine tests on "isolated" and "attached" pads to check the agreement of the results. The term "isolated pad" refers to samples on which the collagenous connections between the calcaneus and the pad have been cut, which allows the analysis of the fat tissue without the bone. On the second group, "attached pads", most of the calcaneus and the heel pad is still attached to the skin on the sides and lower surface of the amputated foot. This configuration tends to preserve the fat chambers, preventing loss of adipose liquid when compressed.

Figure 2.14 shows load-deformation curves for two attached heel pads submitted to pendulum and materials testing machine tests. The authors could evidence that the same sample responded similarly on both tests, predominantly on the loading phase. Therefore, this study could answer the first issue regarding the method.

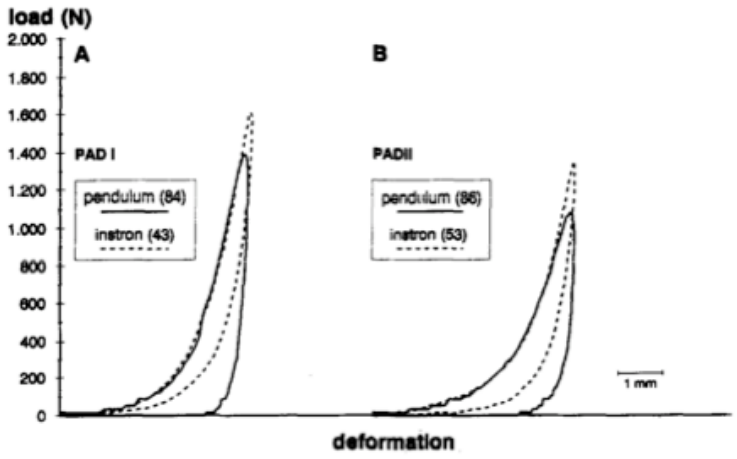

FIGURE 2.14 – Superposition of pendulum and materials testing machine (Instron) tests on two (PAD I and PAD II) attached heel pads (Aerts et al., 1995).

The second question was clarified testing the effect of gradually "isolating" the fat pad, when cadaveric samples were submitted to a series of pendulum or materials testing machine procedures and sequentially freed from the foot. The samples behavior was almost identical, regardless the amount of isolation, as seen on load-deformation curves in Figure 2.15. However, when the pad was completely detached from the calcaneus bone, as shown in Figure 2.16, the curves do not have the same load pattern, evidencing that a system involving the calcaneus bone was necessary to best characterise the structural properties of the heel pad.

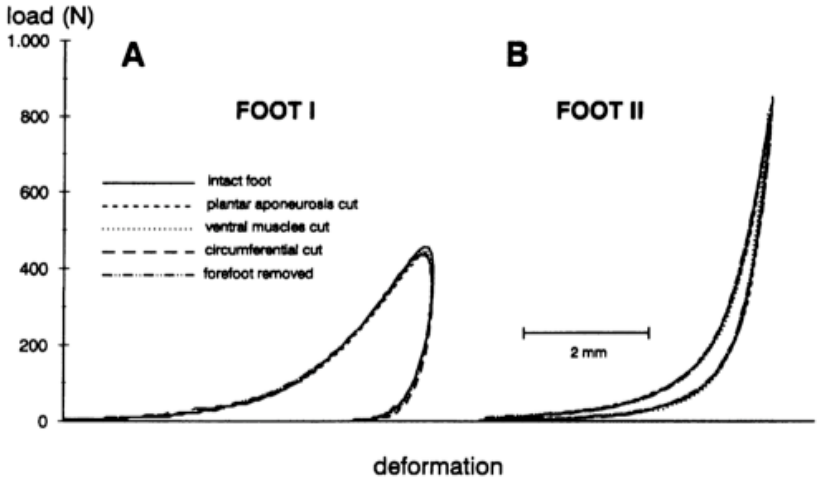

FIGURE 2.15 – Superposition of load-deformation curves of heel pads at different stages of isolation. FOOT I was submitted to a pendulum test and FOOT II was tested on a materials testing machine. (Aerts et al., 1996).

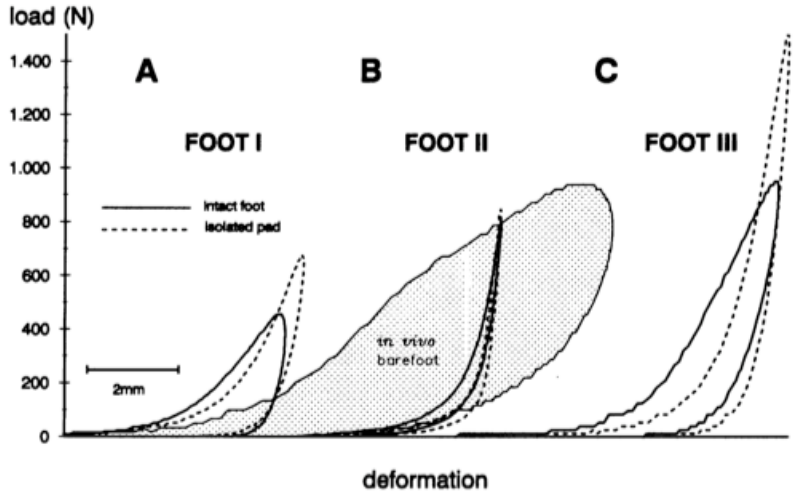

FIGURE 2.16 – Superposition of load-deformation curves of heel pads at two stages, intact foot and isolated pad. FOOT I and FOOT III were submitted to a pendulum test and FOOT II was tested on a materials testing machine. (Aerts et al., 1996).

Therefore, the results obtained by Aerts et al. (1995; 1996) proved that under controlled testing procedures, both pendulum and materials testing machine methods could be applied. Moreover, the use of attached pads best describes the behavior of the human leg system.

In general, when pendulum tests are administered, the EDR tend to be higher than using the materials testing method, and the stiffness is less. This can be explained by the lack of repeatability of the pendulum test. A planar impact and rebound area on the heel does not exist, due to the irregular surface of the plantar pad. Consequently, the pendulum might have its linear movement affected, compromising the results. Aerts et al. (1995) and Ker (1996) supported this hypothesis. They added "preconditioning", where cycles of loading-unloading with a controlled resting period where performed on a materials testing machine, overcoming the single cycle executed on a pendulum test. Therefore, the materials testing machine seems to provide the best results when testing *in vitro* samples, and Table 2.1 summarizes quantitative data acquired using this method from the studies mentioned in this section.

TABLE 2.1 – The mean (SD) stiffness and energy dissipation ratio (EDR) reported for cadaveric heel pads using a materials testing machine approach.

Study	**N**	**Stiffness (kNm^{-1})**	**EDR (%)**
Bennet and Ker (1990)	5	1160 (170)	28.6 (6.9)
Aerts et al. (1995)	9	905 (33)	48.2 (1.8)
Aerts et al. (1996)	2	504 (19)	34.6 (2.0)
Ker (1996)	3	1030 (56)	29.0 (4.1)

N, number of heel pads analyzed.

2.4.2. *In vivo*

The measurements *in vivo* have generally been conducted using non-invasive methods such as indentation, ultrasound, and movement analysis, or minimally invasive tests like X-rays and fluoroscopy. On both approaches, the heel pad structure, characterised by its thickness, and structural properties such as compressibility index (CI), stiffness, and energy dissipation ratio (EDR), are frequently reported. This section presents a summary of the very papers and the results they provided.

2.4.2.1. Thickness and Compressibility Index (CI)

Amongst all measurements done on *in vivo* heel pad tests, unloaded thickness is by far the most reported characteristic, regardless of the method used. It is based on a measure of the shortest distance between the lowest portion of the plantar tuberosity of the calcaneum and the skin edge (Hsu et al., 1998; Turgut et al., 1999; Uzel et al., 2006b), in both unloaded and loaded setups. These two values are used to calculate the compressibility index, and a secondary benefit provided by the measurement of these values is that they give the basis of two important derived properties, stiffness and EDR.

Thickness and CI have been reported in healthy individuals and associations made with age, gender and ethnic origin (Bohrer and Ude, 1978; Prichasuk, 1994). In addition, some few conditions such as diabetes and plantar heel pain have also been investigated and these properties compared with healthy controls (Kanatli et al., 2001; Erdemir et al., 2006).

To provide a deeper description of the studies that reported these properties, a classification according to the methods used was chosen, although the results do not differ in a great extent amongst them when similar conditions were applied.

X-ray studies

Radiographic investigations had been used largely, and several publications yielded fundamental results, even after the advent of less invasive techniques. Due the radiation emission and the magnification effect characteristic of this method, its use decreased lately, being overtaken by cheaper and non-invasive methods, like ultrasound or indentation (Uzel et al., 2006b).

However, two studies have used large groups of healthy subjects on its investigations. Prichasuk et al. (1994) found a greater thickness in a group of 200 men compared to the same number of women, and the thickness also increased with age (Table 2.2). These findings do not support previous work done by Bohrer and Ude (1978), who analyzed 343 black individuals in Nigeria and found no differences regarding gender or age. Their results show, on the other hand, an increased thickness when compared with an American black population. Ethnic characteristics probably have influenced the discrepancies between the results of these two studies, however the benefit of researches with a large sample is certainly a better representation of that particular population.

When contrasting groups of healthy people and patients with plantar heel pain (PHP), Prichsuk (1994) found significant differences in thickness and the CI, with increased values for the PHP patients and also for healthy men compared with healthy women. The same findings were not corroborated by Turgut et al. (1999), when dissimilar subgroups were analyzed (weight, gender, age, body mass index) and no differences have been found. This subdivision approach can give better results, since comparisons are restricted to people with similar characteristics. Kanatli et al. (2001) also has not found any difference in thickness and CI between PHP and healthy controls, and raised doubt over the clinical use of the CI as a diagnostic tool.

This questioning is justified by the lack of a conclusive investigation on the expected values for the CI, either on a healthy population or individuals with some clinical abnormally. As a ratio between the loaded and unloaded thickness, it is supposed that values near 1 represent a completely rigid heel pad, without any ability to deform under body weight loading. As shown in Table 2.2, the CI range is 0.4 to 0.7, which generally represents a material with capacity to reduce its size by half, even for patients with PHP. Therefore, the use of CI as a diagnostic tool is still a matter of debate.

Table 2.2 summarizes findings of the studies mentioned. It is fair to compare the data, as all have used the same radiograph settings: tube-film distance of 40 inches, using 45 kV and 5 MAS (125 mA, 0.04 sec).

TABLE 2.2 – The mean (SD) unloaded thickness, loaded thickness, deformation, compressibility index (CI), and subject condition reported for in vivo heel pads and measured with X-rays.

Study	Unloaded thickness (mm)	Loaded thickness (mm)	Deformation (mm) †	CI	Condition
Bohrer and Ude (1978)	22.2 (2.8)	N/A	N/A	N/A	Healthy
Prichasuk et al. (1994)	19.3 (2.4) (M) § 18.0 (2.2) (F) §	10.3 (2.2) (M) 9.5 (2.3) (F)	9.0 (M) 8.5 (F)	0.53 (0.09) (M) 0.53 (0.10) (F)	Gender
Prichasuk et al. (1994)	18.3 (2.4) (G1) § 19.0 (2.4) (G2) §	9.4 (2.3) (G1) 10.5 (2.2) (G2)	8.9 (G1) 8.5 (G2)	0.51 (0.09) (G1) § 0.55 (0.09) (G2) §	Age
Prichasuk (1994)	18.7 (2.3) (C) § 20.6 (2.5) (P) §	9.8 (2.2) (C) § 12.1 (2.6) (P) §	8.9 (C) 8.5 (P)	0.52 (0.08) (C) § 0.59 (0.10) (P) §	PHP
Turgut et al. (1996) *	18.5 (2.1) (C) 18.2 (3.1) (P)	7.8 (1.7) (C) 8.4 (2.1) (P)	10.6 (C) 9.8 (P)	0.41 (0.09) (C) 0.46 (0.10) (P)	PHP
Kanatli et al. (2001)	19.5 (2.5) (C) 20.4 (2.8) (P)	11.8 (2.8) (C) 14.0 (3.3) (P)	7.7 (C) 6.4 (P)	0.60 (0.11) (C) 0.69 (0.14) (P)	PHP
Uzel et al. (2006a)	20.0 (2.6) (P)	12.5 (2.8) (P)	7.5 (P)	0.62 (0.09) (P)	PHP

N/A, not available; P, patient group; C, control group; PHP, Plantar Heel Pain; *, subjects younger than 40 years old with normal weight; M, males; F, females; G1, healthy subjects between 20-35 years old; G2, healthy subjects between 40-60 years old; †, calculated values; §, statistically significant difference.

Ultrasound studies

The ultrasound method of measure heel pad thickness has been preferred over X-rays, because it has not got the inherent problem of radiation, neither provide the magnification effect on the images. It is portable, easy to use and reliable. This was evidenced by Uzel et al. (2006b), who compare the ultrasound technique with radiographs. They have taken images from the fat pad using both methods and reported a strong positive

correlation between them, which makes the equipment a good choice for heel pad studies. The negative aspect of the ultrasound is it "operator-dependable" characteristic, that make it a device that requires experienced personnel to operate it.

When used independently of any additional tool to measure loadings (indentation devices use it in general), ultrasound can measure the heel pad in two situations: unloaded and loaded. However, differently from X-ray tests where the subjects measured under body weight loading simply stand on a platform and compress the entire heel, the ultrasound probe generally is thinner than the heel width. Therefore, compress the probe against the heel, or on opposite, might led to different compression patterns that those obtained by radiographic investigations. To avoid this restriction, researchers use custom made devices that incorporate the ultrasound probe into them, one of them is shown in Figure 2.17. Some devices have embedded load cells that can record the amount of force exerted on them, which enable the system to emit a sound when a specific load has been reached (Hsu et al., 2007). Unloaded measurements, on the other hand, do not need a special device, the probe is generally held by the operator, with the subject laid prone.

FIGURE 2.17 – Ultrasound method to exam the heel pad thickness. The ultrasound probe is placed under a slot in a wooden platform. (Uzel et al., 2006b).

Healthy subjects had their heel pads measured by Rome and colleagues (Rome et al., 1998b) and the mean deformation (unloaded thickness minus loaded thickness) reported was 8.40 mm. This value goes in accordance with previous radiologic studies, as seen in Table 2.2, however results for unloaded thickness are very dissimilar (Table 2.3). This perhaps is a consequence of the method used to collect these images. The probe is held by an operator, and cannot compress the plantar surface, otherwise some initial deformation will happen, compromising the measurement. This same device and method was used again on a larger study (Rome et al., 2002), however unfortunately the authors they did not report values for unloaded thickness and deformation, restricting comparisons with other works. In this study patients with PHP showed a higher deformation compared to controls.

A more comprehensive study was made by Uzel et al. (2006b), when heel pad structure was measured in healthy adults with and without athletic activity. The strongest point is the amount of subjects, 110 in total, distributed into three groups, with both feet measured, however, the results (Table 2.3) did not yield any difference amongst the groups. These researchers also reported values to a group of PHP patients in a study comparing X-ray and ultrasound methods (Uzel et al., 1996a).

A different approach was made by Hsu and colleagues in two studies (Hsu et al., 2007; Hsu et al., 2009). They did more than measure the unloaded and loaded thickness of the entire heel pad, the authors reported the behavior of internal layers, the microchambers and macrochambers. On the first study, a pilot investigation evaluated how differently these layers compress in healthy volunteers, and associated it to the internal distribution of small chambers next to the skin (microchambers) and greater chambers deeper in the pad (macrochambers). Figure 2.18 shows how these layers were measured on the ultrasonographic image. They concluded that the macrochamber layer is responsible for more than 95% of the total deformation, which, according to the authors, provides “a treatment guide of

injection of viscous supplement for reducing risk of tissue breakdown in diabetic patients" (Hsu et al., 2007).

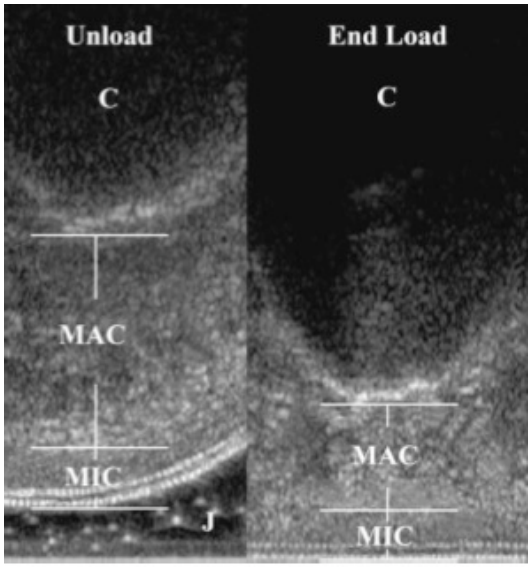

FIGURE 2.18 – Ultrasound image of the heel pad on load and unloaded conditions. Microchambers (MIC) and macrochambers (MAC) can be identified, and also the calcaneus bone (C) and the acoustic gel (J). (Hsu et al., 2007)

To extend the method to a greater population, the authors investigated the structural properties of the layers in diabetes patients (Hsu et al., 2009). A total of 29 diabetic heels were compared with an age-matched group and values for loaded and unloaded thickness reported, and although they have not found significant difference in these values for the heel as a whole, macrochambers in diabetes patients have deformed less. This might be associated with an increase in the fibers that compose the septal walls, limiting the resilience, but no evidence was found in literature. This study shows how the ultrasound method can extrapolate the barriers of the analysis of the heel pad as a unique entity, and pointing out the heterogeneous characteristics of this tissue.

TABLE 2.3 – The mean (SD) unloaded thickness, loaded thickness, deformation, compressibility index (CI), and subject condition reported for in vivo heel pads and measured with ultrasound.

Study	Unloaded thickness (mm)	Loaded thickness (mm)	Deformation (mm) †	CI	Condition
Rome et al. (1998a)	12.4 (4.2)	4.0 (1.8)	8.4	0.33 †	Healthy
Rome et al. (2002)	N/A	5.02 (1.4) (C) 5.75 (1.1) (P)	N/A	N/A	PHP
Uzel et al. (2006a)	18.6 (2.5) (C1) 18.0 (2.0) (C2) 18.2 (2.4) (C3)	11.3 (1.9) (C1) 10.4 (1.5) (C2) 11.0 (2.1) (C3)	7.3 (C1) 7.6 (C2) 7.2 (C3)	0.61 (0.06) (C1) 0.58 (0.05) (C2) 0.60 (0.05) (C3)	Athletic activity
Uzel et al. (2006b)	19.8 (2.9) (P)	12.3 (2.9) (P)	7.5 (P)	0.62 (P) †	PHP
Hsu et al. (2007)	14.7 (2.2)	8.8 (0.8)	5.9	0.60 †	Healthy
Hsu et al. (2009)	18.4 (1.2) (C) 19.3 (3.0) (P)	12.8 (C) † 11.7 (P) †	5.6 (C) 7.6 (P)	0.69 (C) † 0.61 (P) †	Diabetes

N/A, not available; P, patient group; C, control group; PHP, Plantar Heel Pain; †, calculated values; C1, sedentary group; C2, low athletic activity group; C3, high athletic activity.

Indentation studies

Radiographic and ultrasound equipments are able to collect useful images to measure heel pad thickness, however when the attention goes to the analysis of stiffness and EDR these equipments alone cannot provide the necessary information. In addition to the deformation, or how the thickness changes over time, the loading applied to the heel has to be measured as well. Indentation studies are most used to this aim, and thickness and CI are also been reported with this method.

Two studies using the same indentation device (Hsu et al., 1998; Tsai et al., 1999), which consists of a manual compression-relaxation system connected to an ultrasound probe (see Figure 2.7a), reported results with this method. The equipment applied serial increments of 0.5 kg to the heel being tested, reaching a maximum of 3 kg, followed by similar decrements. All the measures were taken at a speed of 0.0006 m/s, very low compared to the normal walking impact velocity of 0.52 m/s (Chi and Schmitt, 2005), which characterizes the experiments as quasistatic.

Initially, young and elderly healthy subjects were investigated. They found a significant increase both in unloaded thickness and CI on the group more than 60 years old, reinforcing the findings of a radiographic study on a large healthy population (Prichasuk et al., 1994). These results might not be affected by the speed differences between the quasistatic test and the real impact velocity, because the CI is based on the final or maximum loaded thickness, but can be questioned regarding the load applied. The indentation method generally uses low maximum loads, 3 kg in this case, to avoid any damage to the ultrasound probe, therefore the results for the CI tend to be greater then those obtained under body weight loading. The pressure applied by the transducer, according to the authors, was "close to the peak in-sole plantar pressure in the heel region of healthy individuals" (Hsu et al., 1998), however this fact does not eliminate the concentrated compression of the heel at the probe location. The heel soft tissue located beside the ultrasound transducer is under a different compression pattern, and might contribute to the some difference on the values, when compared to other methods. However, even with this restriction, the findings suggest different tissue behavior in older adults.

Similar results were not reported when a group of unilateral plantar heel pain (PHP) patients had these properties of their affected heel compared to their contralateral heel used as a control group (Tsai et al., 1999). Table 2.4 shows the results of this research. These two studies used the same device and procedure to collect and compare data from different populations, and although the results point to similar trends to other methods (Turgut et al., 1999; Kanatli et al., 2001), no further investigation was undertaken to validate

the tool. Unfortunately, the lack of methodological research to validate equipment like this indentation device limits the power of some findings.

TABLE 2.4 – The mean (SD) unloaded thickness, loaded thickness, deformation, compressibility index (CI), and subject condition reported for in vivo heel pads and measured with indentation devices.

Study	Unloaded thickness (mm)	Loaded thickness (mm) †	Deformation (mm) †	CI	Condition
Hsu et al. (1998)	17.6 (2.0) (G1) § 20.1 (2.4) (G2) §	9.3 (G1) 12.2 (G2)	8.3 (G1) 7.9 (G2)	0.53 (0.08) (G1) § 0.61 (0.05) (G2) §	Age
Tsai et al. (1999)	18.2 (2.4) (C) 17.6 (2.9) (P)	10.7 (C) 10.3 (P)	7.5 (C) 7.3 (P)	0.59 (0.07) (C) 0.59 (0.06) (P)	PHP

P, patient group; C, control group; PHP, Plantar Heel Pain; †, calculated values; G1, healthy adults with less than 40 years old; G2, healthy adults with more than 60 years old; §, statistically significant difference.

Movement Analysis study

Gait analysis uses equipment that collects two and three-dimensional data. However the equipment is not generally the first choice when small movements must be evaluated. This is shown by the lack of evidence that these systems can obtain reliable data from fast and small displacements.

There were no studies using 3D movement analysis to evaluate how the heel pad deforms, not only in the sagittal plane or vertical direction, but also how it expands medio-laterally and posteriorly under loading. Only one investigation used this type of system to evaluate thickness of the heel pad in one direction (Chi and Schmitt, 2005). Amongst several types of data collected (reaction forces, foot mass, velocities, accelerations), the authors also used a movement analysis system to gather the vertical deformation of the heel pad using one 3 mm hemispherical reflective marker (Figure 2.19). The study did not give the results neither for unloaded nor loaded thickness, only deformation values were reported, which limits the comparison with

other methods. At normal walking speed (approximately 1.6 m/s) the heel pad deformed by 5.24 ± 1.23 mm, a value almost 40% less than those found with ultrasound (Rome et al., 1998b). Despite this difference, the work pioneered the use of this method to report soft tissue deformation.

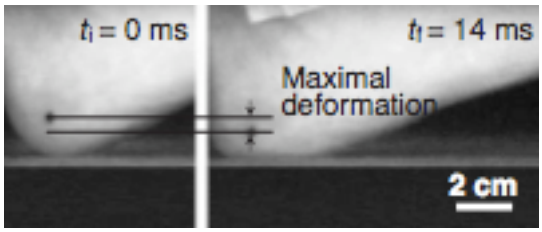

FIGURE 2.19 – 3 mm hemispherical marker attached to the heel pad to collect deformation values using a three-dimensional movement analysis system. (Chi and Schmitt, 2005).

Fluoroscopy studies

In order to provide stress-strain relationships, Gefen and colleagues employed an integrated method to measured heel pad thickness using fluoroscopy and the applied stress using a pressure platform (Gefen et al., 2001). In addition to these two variables, elastic and viscous parameters of the tissue were also used to compose a constitutive model that described the stress-strain relationships. EDR and modulus were the main outcomes of this study. However thickness and deformation were also reported. They observed two healthy participants walking at low velocities (0.5 m/s to 0.9 m/s), and compared this to other studies with different methods, the values published were smaller than those reported with different methods (Table 2.5), which might be explained by the low number of participants.

A similar approach was used in a different study investigating the differences between two groups: asymptomatic and plantar heel pain subjects (Wearing et al., 2009). Comparisons between structural properties of the heel pad in both patient and control groups showed no statistical significant difference in unloaded and loaded thickness (Table 2.5). The

authors used a fluoroscopy to acquire values for thickness and deformation and a plantar pressure platform to gather the stress applied to the heel pad when walking. The technique adopted has the advantage to correct spatial distortions that occur on the fluoroscopic field of view using a calibration grid, which might lead to more accurate values to the thickness. Stiffness and EDR were also observed and will be described in the following sections.

TABLE 2.5 – The mean (SD) unloaded thickness, loaded thickness, deformation, compressibility index (CI), and subject condition reported for in vivo heel pads and measured with fluoroscopy.

Study	**Unloaded thickness (mm)**	**Loaded thickness (mm)**	**Deformation (mm)**	**CI**	**Condition**
Gefen et al. (2001)	11.2 (0.2) (C1) 13.1 (0.2) (C2)	7.4 (C1) † 8.3 (C2) †	3.8 (0.5) (C1) 4.8 (0.5) (C2)	0.66 (C1) † 0.63 (C2) †	Healthy
Wearing et al. (2009)	19.1 (1.9) (C) 19.3 (1.7) (P)	8.8 (1.5) (C) 10.0 (2.1) (P)	10.3 (C) † 9.3 (P) †	0.46 (C) † 0.52 (P) †	PHP

P, patient group; C, control group; PHP, Plantar Heel Pain; †, calculated values; C1, healthy subject 1; C2, healthy subject 2.

2.4.2.2. Stiffness

When both load and deformation values are collected, the stiffness can be calculated by dividing the first by the second. The reported value represents the resistance of the tissue to deform under an applied force. Therefore high values indicate a body less prone to compress. However, when tissues like the heel pad are submitted to loading and unloading cycles, they respond in a non-linear way, with forces rising more rapidly with increasing deformation, as shown in Figures 2.14, 2.15, and 2.16, section 2.4.1., and there is no agreement in the literature on what portion of the load-deformation curve best represents this property.

In vitro studies reported stiffness varying from 504 to 1160 kN/m, when loading heel pad samples up to 1400 N (Table 2.1). However the values were calculated using different parts of the curve. Bennett and Ker (1990) used load and deformation values correspondent to body weight, whereas Aerts et al. (1995) calculated the stiffness over the loading range between 700-800 N. In another study, the same group (Aerts et al., 1996) used a lower range to the calculation: 200-400 N. It is evident that the results obtained cannot be compared, as the slope of the load-deformation curve being assessed is completely different amongst the experiments. Unfortunately the same lack of comparison criteria is found in *in vivo* investigations, in addition to a great variance on the load applied.

Using an impact testing method, Aerts and de Clercq (1993) observed how different shoes influence the heel pad compression behavior. They used data from 9 healthy subjects, in which heels were impacted by a pendulum device under loads from 600 to 1000 N, simulating impact velocities varying from normal walking to running. They also measured barefoot conditions, in order to have baseline parameters to compare, under the same setup. Figure 2.20 shows the curves obtained to the latter situation, where each curve represents a different impact velocity.

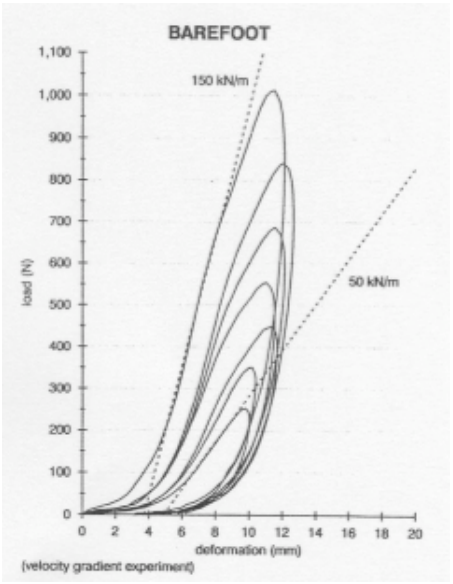

FIGURE 2.20 – Load-deformation curves obtained during impact testing. The dashed lines represent the final stiffness (linear regression) of the 0.37 and 0.96 m/s cycles. (Aerts and de Clercq, 1993).

The authors tried to find a linear part of the curve to derive the linear regression and obtain the stiffness, without any load constraint such as total body weight or specific percentage of the maximum loading. This restricts the analysis, since the values acquired might reflect different tissue conditions (Table 2.6). However, it is worth noting that the curves show an increasing slope as the loading increases, suggesting a higher stiffness under elevated loads.

A different approach was given by de Clercq et al. (1994) in a cineradiographic study, where they equally divided the load-displacement cycle into three parts, and reported stiffness results for the first and last thirds. Using it, it was possible to establish a stiffness value to the period when the heel pad deforms the most, the initial third, and another when the curve reaches its maximum slope. The results showed an increase of almost 5 fold in stiffness, when comparing the initial and final moments of compression (Table 2.6). Although the study aim was a characterisation of the heel properties in running with shoes, the segmented stiffness analysis had contributed to a deeper understanding of the functionality of this tissue. The increase in stiffness after a relatively easy initial compression makes

distinctive the non-Hookean behavior, as the more load applied, the stiffer the tissue, which illustrates the bone protection functionality of the heel pad.

Indentation methods are also used to report stiffness. However, since the loads applied by these devices are quite small compared to body weight loads, and also the load rate differ significantly from those applied using other methods, generally the results are also smaller. Hsu et al. (1998) and Rome et al. (2001) tested subjects using maximum loads of 2 or 3 kg, respectively, and both calculated the stiffness dividing the maximum load by the maximum displacement. The results were very similar, as shown in Table 2.6, irrespective of the subject type they studied, but are more than 15 times less than the minimum values reported by Aerts and de Clercq (1993), and more than 40 times less than the initial loading described by de Clercq et al. (1994). Therefore, stiffness results obtained by indentation tests are remarkably lower than those reported using body weight loads.

TABLE 2.6 – The mean stiffness reported for in vivo heel pads, according to the method used to collect data.

Study	**Stiffness (kN/m)**	**Method**
Aerts and de Clercq (1993)	52 (walking velocity) 150 (running velocity)	Impact test
de Clercq et al. (1994)	135 (initial third) 634 (final third)	Cineradiography
Hsu et al. (1998)	3.68	Indentation
Rome et al. (2001)	3.22	Indentation

2.4.2.3. Energy Dissipation Ratio (EDR)

The energy dissipated by the heel pad after a full compression-extension cycle is associated with the loading applied, the rate this load is administered, and also the deformation obtained (Aerts et al., 1995). This fact is clear when comparing the results from several studies carried out with different methods. Impact tests generally are executed under high loading rates, while indentation devices can normally apply low peak loads on quasistatic procedures. Fluoroscopic exams, on the other hand, try to evaluate the heel pad under normal walking conditions, however only a few studies were conducted with this approach.

The EDR results must be interpreted as an indicator of the tissue hysteretic behavior. Therefore, the area between the loading and unloading curves on load-deformation graphs represents the hysteresis loop, which does not exist or is very small on elastic solid materials and is large in inelastic ones. Low values of EDR for heel pads reveal a tissue where the unloading curve is close to the loading curve, thus with a high rebound ability, characterising a more resilient tissue. On the other hand, an extended time to recover its shape increases the distance between the curves, elevating the EDR (Hsu et al., 2000).

In vitro testing using materials testing machines obtained EDR ranging from 29% to 48%, meaning that less than half of energy absorbed during the loading phase was dissipated (Table 2.1). These values are quite low compared to those found in pendulum *in vitro* tests: 65%-86% (Aerts et al., 1995) and 89% (Aerts et al., 1996), confirming that both different loads applied and loading rates are important factors to justify the differences between methods. Supporting these latter findings, Kinoshita et al. (1996) reported a significant difference between EDR in young and elderly people, as shown in Table 2.7. Impact tests were performed on these groups and they found EDR values as high as *in vitro* pendulum testing, at velocities compared to walking and running activities. It is still uncertain, but some authors suggest a "lower leg effect" as the responsible to high EDR values,

where the whole leg absorbs the pendulum impact at various levels (soft tissue, cartilage, joints), which is not observed when quasistatic tests are conducted at the heel pad tissue level, therefore reducing the EDR (Aerts et al., 1995; Tsai et al., 1999).

Three studies used the same indentation device attached to an ultrasound probe under similar loading and unloading regimen to obtain heel pad characteristics from different groups. The maximum load was 3 kg, reached by increments of 0.5 kg, the same occurring at the unloading phase. This quasistatic process using slow loading rates lead to results (Table 2.7) close to those obtained on *in vitro* tests with materials testing machines. Hsu et al. (1998) reported an increased EDR on healthy elderly people compared to a young control group, and the same behavior was found to diabetes patients compared to healthy controls by Hsu et al. (2002). No significant difference were found by Tsai et al. (1999) in a study involving plantar heel pain patients, however the values for EDR were still under the same range. Ruptures or fragmentation of elastic fibers that compose the fat globules wall may explain these results. Microscopic analysis revealed that atrophic heel pads have this architectural structure changed and suggests this causes the loss of tissue resilience (Buschmann et al., 1995).

Plantar heel pain was the group of interest for Wearing et al. (2009), who using a fluoroscopic and plantar pressure method obtained stress-strain curves and could derive EDR values (Table 2.7). As they analyzed patients and controls walking at self-selected speed, the study introduced one considerable difference on the load and loading rate compared to previous investigations. This was evidenced by higher values obtained, ranging from 55% to 69%, with the patient group showing the lower amount of energy dissipated. To justify this finding, the authors suggest that alteration in collagen fibers is influenced by its protein structure (size, quantity, aggregates) and the cohesion of the collagen network, and it might happen on plantar heel pain patients. However, a point to consider is that there is not yet a proven cause-and-effect relationship, i.e. “whether plantar heel pain results in altered properties of the heel pad, or whether reduced energy

dissipation of the heel pad contributes to the development of plantar heel pain" (Wearing et al., 2009).

Similar method have been used by Gefen et al. (2001), by means of an integrated fluoroscopic and plantar pressure device. However, the results represent the lowest values to EDR found in the literature, 18%. This may be a consequence of the inclusion of only two subjects in the analysis, and also by the low stress obtained on the walking cycles (which were performed at low speed, but yielding a high loading rate). Values to deformation were also under those reported at the section 2.4.2.1., corroborating these unusual EDR findings.

TABLE 2.7 – The mean (SD) EDR and subject condition reported for in vivo heel pads, and the method used to collect data.

Study	**EDR (%)**	**Condition**	**Method**
Kinoshita et al. (1996)	76.5 (2.7) (C) § 72.6 (2.5) (P) §	Age	Impact test
Hsu et al. (1998)	23.7 (6.9) (G1) § 35.3 (10) (G2) §	Age	Indentation
Tsai et al. (1999)	31.8 (10.7) (C) 32.6 (11.9) (P)	PHP	Indentation
Hsu et al. (2002)	27.9 (6.1) (C) § 36.1 (8.7) (P) §	Diabetes	Indentation
Gefen et al. (2001)	17.8 (0.8)	Healthy	Fluoroscopy
Wearing et al. (2009)	69 (8) (C) § 55 (17) (P) §	PHP	Fluoroscopy

P, patient group; C, control group; PHP, Plantar Heel Pain; G1, healthy adults with less than 40 years old; G2, healthy adults with more than 60 years old; §, statistically significant difference.

Summary

Several methods have been used to collect thickness, deformation, CI, stiffness, and EDR values from the heel pad. The large list of differences amongst these methods, such as health hazards, cost, user dependant analysis, inherent machinery distortions, amount of loading, velocities, amongst others, prevent a fair comparison between studies. However, the great majority describes values for these structural properties under a range of 12-20 mm for unloaded thickness, CI ranging from 0.4-0.7, and a deformation on the coronal plane of 4-12 mm for healthy subjects.

Stiffness results depend on the portion of the load-displacement curve analyzed, therefore reported values range from 52-630 kN/m. A great variation is also observed on EDR, where the load amount, loading rate, and the method used to collect data seem to influence the results the most, with values ranging from 23-69%.

Further work is therefore justified to establish heel pad properties under weight bearing conditions and in three-dimensions. The aim of this study was therefore to validate a method of measuring the three-dimensional forces and deformations of the heel pad *in vivo*, use this method to investigate heel pad properties in healthy individuals, and evaluate the influence of gender on the results.

However, in order to evaluate the ability of motion analysis system to collect displacements of the magnitude of heel pad deformation observed in the literature, a pilot study needed to take place. The next chapter describes the procedure adopted to assess these system capabilities by the use of compressible probes, which helped designing of the human test protocol, detailed in chapter 4.

3. Silicone Testing

The first objective of this work was to evaluate the ability of the Movement Analysis System to measure small deformations, as those found on the human heel pad under compression. Stereophotogrammetry systems are tools that have already been validated to quantify gait (Kadaba et al., 1989), where reflective markers, generally of 14 mm in diameter, are placed on the skin and its movement is translated into three-dimensional coordinates. In gait measurements, displacements in the range of 10 mm (the vertical deformation of the heel pad) are acceptable and in most cases do not compromise the results. However modern systems are theoretically accurate to 1 mm or less. It was necessary therefore to investigate the magnitude of systematic and random errors associated with the system to establish if it was capable of measuring the heel pad deformations.

This chapter describes a pilot protocol designed for this task, the results obtained, and examines how they can influence the measurements of heel pad deformation.

3.1. Introduction

The protocol chosen to evaluate the accuracy of the motion analysis system to measure small deformations was the comparison of the results obtained using this equipment to collect displacements and a force platform to gather load values with data acquired in similar conditions on a materials testing machine. Three samples made of cylindrical silicone rubber, each with a different hardness, were submitted to the same loading and unloading procedure using both methods, and the vertical deformation recorded. Considering the materials testing machine as an already established reliable tool to quantify small displacements, a comparison between the results could

be made, indicating if the motion analysis system is also a reliable equipment for such task.

Initially, therefore, it was necessary to understand how the motion analysis system expresses its inherent or systematic errors. Restricting the analysis to the device used in this study, the references to the stereophotogrammetric or motion analysis system are based on the Vicon Motion Analysis equipment (Oxford Metrics, Oxford, UK). In order to understand how it works, some fundamental concepts are reviewed.

Camera calibration and residuals

The cameras used on optical sterophotogrammetric systems are composed by a strobe of infrared lights and a special set of lenses (Figure 3.1). The strobe emits infrared light that illuminates the retro-reflective markers attached to the subjects, and the markers reflect the light back to the camera. There are filters on the lens that allow this particular light to reach the camera sensitive plate, which collects location in field of view information and passes it to the processing software. The system can transform a series of these images into three-dimensional coordinates of each marker in a referenced space. To know exactly where the marker is on this space, the system has initially to calculate the relative location and orientation of all the cameras, and this is done using a process called calibration.

FIGURE 3.1 – Optical stereophotogrammetric camera. IR, infrared strobe sensors; L, camera lens.

The procedure consists of two steps: static and dynamic calibration, where the first calculates the origin of the capture volume and also determines the orientation of this workspace, and the second computes the relative position and orientation of the cameras. The process yields a reference parameter used to evaluate the calibration quality, the camera residual. It is based on the root mean square (RMS) of the distance between the ray from the centre of the strobe ring to the marker centroid and the ray reflected from the marker to the camera lens. Each camera has it own residual, and the mean residual is the mathematical mean of all cameras, therefore the lower the value, the better the calibration, resulting in more accurate measures. According to the manufacturer this value should be less than 0.1% of the distance from the centre of the volume to the camera, which results in residuals for a laboratory of dimensions 10 m X 10 m X 3 m ranging from 1 to 4 mm, for instance.

As described in section 3.2.2., the volume used for this test was 1.2 m long, 0.4 m high and 1.2 m wide, which leads to a recommended residual of less than 1 mm. The calibration executed before all tests generated residuals under this value, as seen in section 3.2.3.

Therefore, the residual value calculated after the calibration process is considered a systematic error associated with the measures obtained with the motion analysis system.

3.2. Methods

3.2.1. Silicone samples

In order to simulate deformations from the same magnitude that obtained during the heel pad compression, a soft material able to be compressed under loading and extend after the loading was removed was needed. There was also the necessity to test the compression of the same material with different hardness, to reproduce the behavior of the heel soft tissue (more or less stiffer) and evaluate whether the equipment could convey this material change in terms of deformation values. Silicone rubber is an elastic polymer easily molded, and produced by the mixture of two parts: a base and a curing agent. By adding a thinner, like acetone, it is possible to dilute the compound and alter its hardness.

Therefore, three cylindrical samples of this material, Silastic 3483 Base and Silastic 83 Curing Agent (Dow Corning, Midland, USA) were made, all with the same dimensions (Ø66 mm X 20 mm), but each one diluted with a different amount of acetone. From the total weight of the mixture of the base silicone and the curing agent of each sample, 2%, 5% and 10% of acetone was added, reducing the hardness of the silicone rubber. Figure 3.2 shows one of the cylindrical samples.

FIGURE 3.2 – Silicone rubber cylindrical sample used to compare the deformation values acquired on Motion Analysis and Materials Testing Machine (MTM) compression tests.

3.2.2. Equipment

Motion Analysis

Three-dimensional movement of a set of 13 hemispherical auto-reflective markers, with a diameter of 3 mm and attached to a bar mounted on a special rig, was captured using a six-camera optical stereometric system (Vicon 612, Oxford Metrics, Oxford, UK), sampling at 120 Hz and employing a capture volume of 1.2 m long, 0.4 m high and 1.2 m wide.

Force data were acquired with one 40 x 60 cm Kistler force platform with four 3-component force sensors (Model 9281C, Kistler Instruments Ltd., Winterthur, CH) connected to a PC via an eight channel Kistler type 9865B charge amplifier. Anteroposterior (X), medio-lateral (Y) and vertical (Z) forces were sampled at a rate of 3000 Hz. The position and force data synchronisation was done automatically following calibrating the motion analysis system.

The silicone compression tests were carried out using a custom made device consisting of an aluminum pole mounted on a metallic support structure. The pole could move vertically on the support, and on its top a circular plate was used as a weight stand. Standard weights could be placed upon this stand to compress a silicone sample positioned at the bottom of the pole, and the rig was placed over a force platform to capture the load exerted during the process, as illustrated by Figure 3.3. The motion analysis cameras were mounted around the rig, on a semicircular shape, to guarantee the visualisation of all 13 markers.

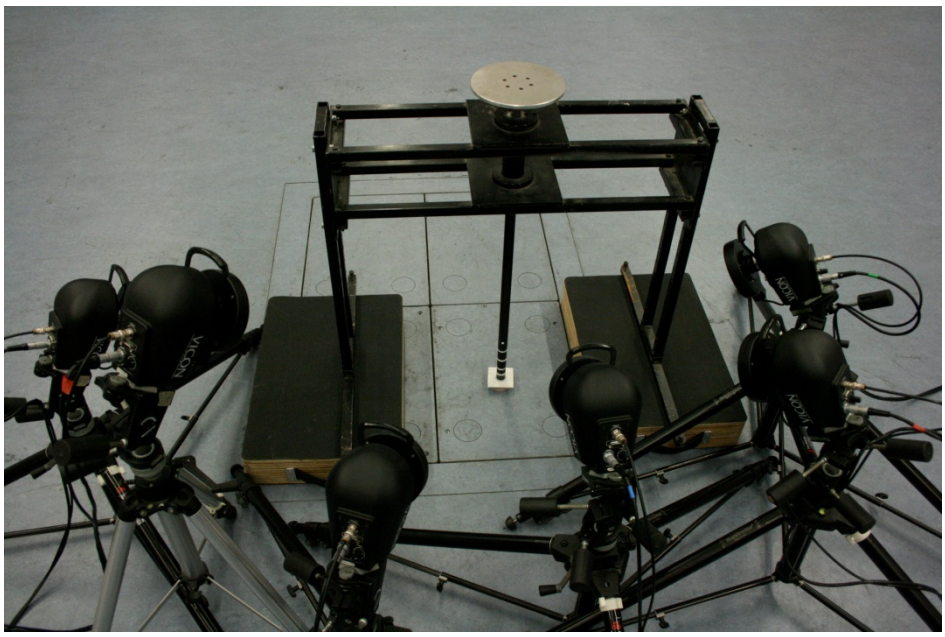

FIGURE 3.3 – Device used on the silicone compression test mounted over a force platform and surrounded by 6 motion analysis system cameras.

A detailed image of the rig is in Figure 3.4a, and Figure 3.4b shows how the reflective markers were positioned on the pole. To uniformly distribute the weight applied on the pole to compress the silicone, a squared metallic plate was used between the bottom end of the rod and the top of the silicone sample (Figure 3.4b). This setup allows the capture of vertical movements, as the pole support could not permit displacements in other directions.

The choice of 13 markers was made based on the same amount to be used on the measurement of the human heel pad deformation. They were placed along the end of the pole on 5 different height levels, four levels with three markers each, separated by 15 mm and the highest level consisting of only one marker. The distance between the rod rim to the first marker level was 20 mm, and the same value between this and the second level; all other vertical distances were 30 mm. No rotational movement was allowed, therefore, no relative displacement amongst the markers was expected, since they were attached to a rigid body.

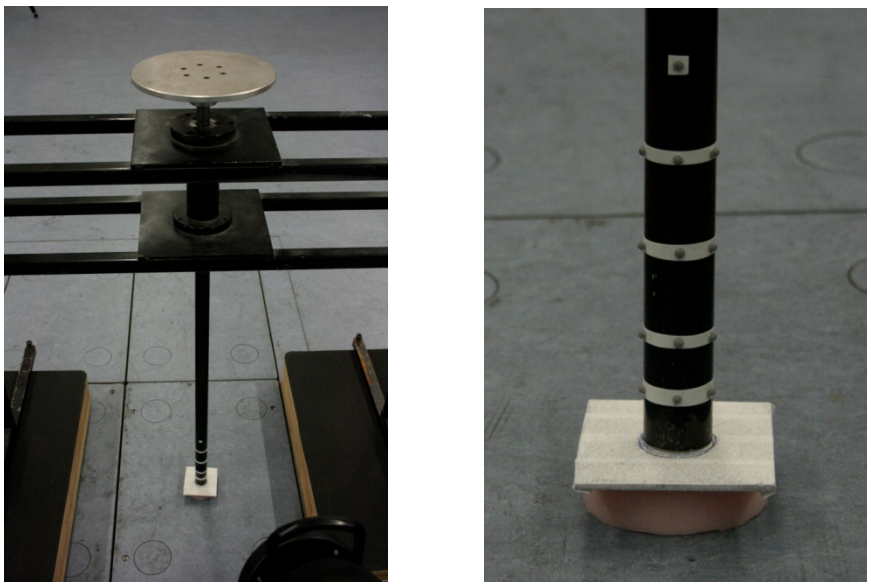

(a) (b)

FIGURE 3.4 – Details of the silicone compression device used in the motion analysis test. (a) Pole and circular weight stand. (b) Hemispherical auto-reflective markers attached on the pole, metallic plate and silicone sample.

Materials Testing Machine

The silicone samples underwent compression cycles on a materials testing machine (Instron Series 5500r, Instron Corporation, Canton, USA). The samples were located between the rigid surface of the cross head and the metallic plate on the load cell, as shown in Figures 3.5a and Figure 3.5b. The moving element of this system was the cross head, which could be programmed to move upwards (loading cycle) and downwards (unloading cycle) using the force readings obtained on the load cell or using a predetermined amount of time.

Vertical displacements were acquired during the tests, and they corresponded to the relative movement between the cross head and the load cell. The acquisition frequency used was 125 Hz.

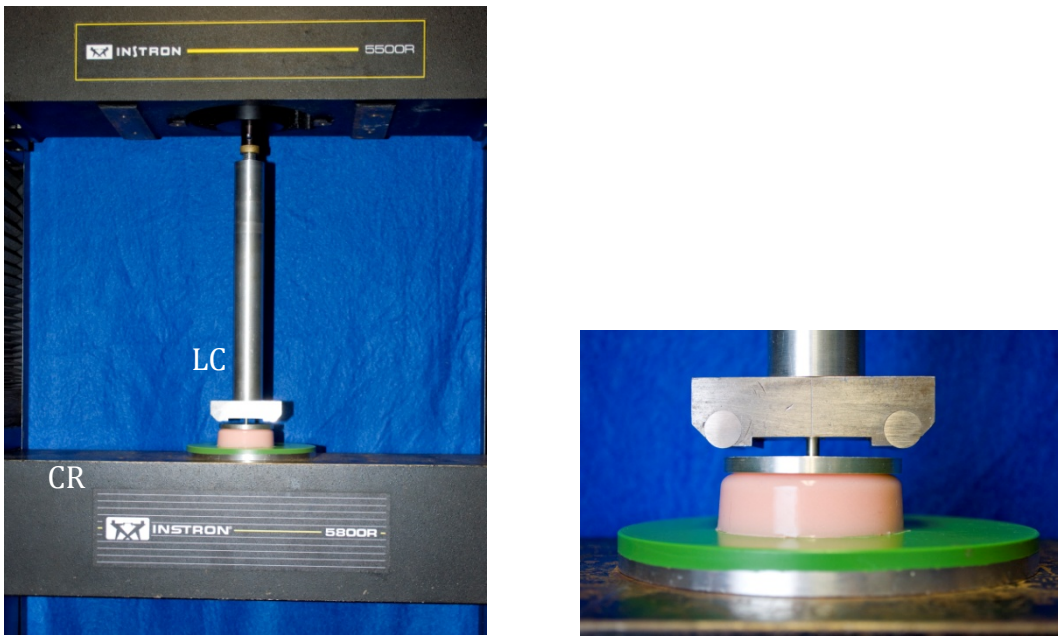

(a) (b)

FIGURE 3.5 – (a) Materials testing machine used in the silicone compression test. (b) Details of the position of the silicone sample being tested. LC, load cell; CR, cross head.

3.2.3. Loading/unloading procedure

All three silicones samples were tested under similar conditions on both motion analysis system and materials testing machine. The samples were initially pre-compressed with a load of 12.2 kg and additional loads of 9.2 kg were implemented on intervals of 10 seconds. This stepwise method was used to minimize the transient effects that occur just after a new loading, stabilising the deformation during the resting period.

The deformation at the pre-compressed point was considered equal to zero, therefore, the displacement obtained from the completely uncompressed position until the pre-load was discarded. The value of 12.2 kg is the weight equivalent of the circular plate and aluminum rod used on the motion analysis rig plus one standard weight plate.

On the motion analysis system, all tests were conducted on the same day, with the system calibrated with a residual of 0.12 mm. The data collection started with the silicone sample pre-loaded and at each 10 seconds, measured using a metronome, a standard weight plate of 9.2 kg was carefully put onto the circular plate stand. The procedure compressed the silicone with 5 subsequent loads and the removal of the standard weighs from the stand provided the unloading cycle. Vertical displacements of the reflective markers on each load level were calculated from the three-dimensional coordinates.

The automatic sequence on the material testing machine was similar, with stepping loading and unloading cycles, and the same resting period between each step. Figure 3.6 shows the pattern of these cycles, exhibiting the forces applied over time.

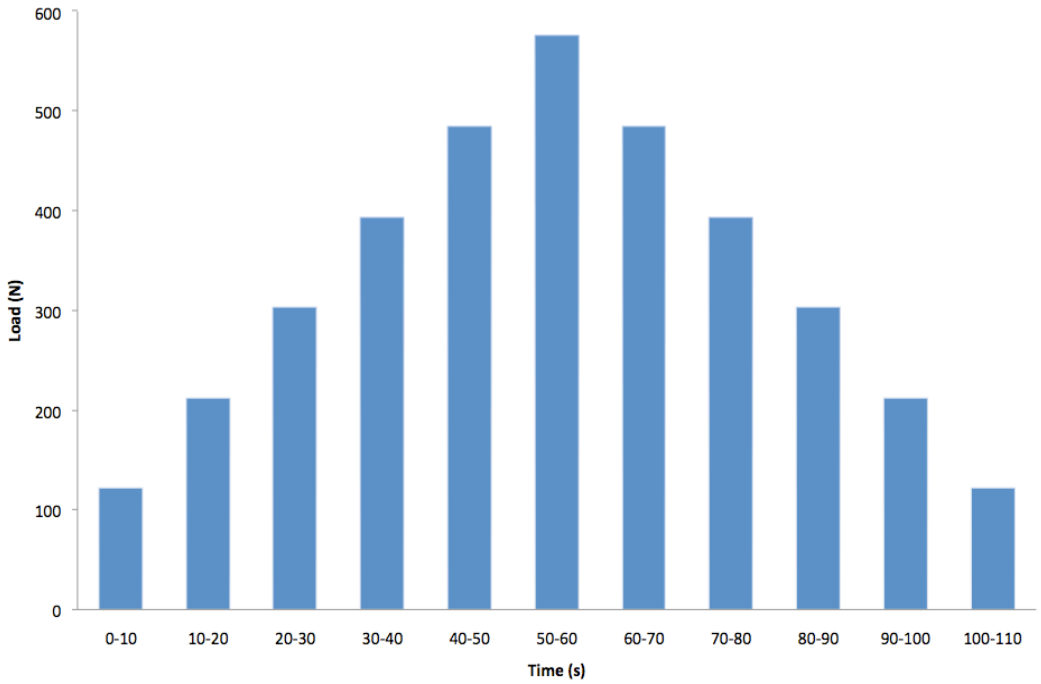

FIGURE 3.6 – Load and unload cycles applied to the silicone samples using both motion analysis system and materials testing machine methods.

On both experiments there was collected one loading/unloading cycle from each silicone sample. As a pilot test, the objective of this comparison between these two methods was to evaluate the magnitude of the discrepancies involving the results, and check whether the motion analysis system shows a trend on these differences, indicating a potential systematic error.

3.2.4. Data analysis

Deformation of the silicone samples was assumed to be equal to the vertical displacement of the moving metallic rod, as seen in Figure 3.4a. The motion analysis system captured the displacement of a set of 13 auto-reflective markers attached to this rod (Figure 3.4b), distributed on five levels along its height. Data was collected with the silicone sample pre-loaded with one standard weight placed onto the rig stand, and the displacement at this moment was considered equal to zero.

During the loading and unloading cycles, as standard weights were added and removed from the rig stand, vertical displacement of each marker was calculated subtracting the Y coordinate component (vertical) at the instantaneous component from the initial position (zero level). Considering that no relative movement occurred among the markers, the vertical deformation of the silicone sample was the average of all individual marker displacement at each moment. For the materials testing machine the data comprises the cross head vertical displacement (Figure 3.5a) and the same pre-load procedure was adopted. Therefore, data from this position relative to all other loading and unloading steps were calculated, and the load information provided by the equipment used to yield load-deformation curves.

For each step on both loading and unloading cycles only the steady load and deformation were used on the analysis. Data from the period when the loading was increasing or decreasing were discarded on both systems due to the manual procedure adopted on the motion analysis system. On the motion analysis test, the process of adding or removing the standard weights onto the rig stand could not be totally controlled, varying in the time used to do the action. Therefore, the results were based on the average of the vertical displacement of all 13 markers and load for the 10 stable seconds on each step. The standard deviation of these values was calculated and was neither

higher than 0.04 mm for the displacement nor higher than 0.85 N for the load.

Stiffness was calculated using the loading portion of the load-deformation curve, from the slope of the linear regression line formed by the data points between 30% and 85% of the maximum load. For both deformation and stiffness analysis the data was processed on Microsoft Excel software (Microsoft Corp., Washington, USA)

The trapezoid rule was used to numerical integrate the loading and unloading curves and work out the area beneath each. Energy dissipation ratio was estimated by the division of the area between these curves (hysteretic loop) by the area of the loading curve (Wearing et al., 2009) using Matlab software (MathWorks Inc., Massachusetts, USA).

To evaluate the influence of the deformation differences on the entire cycle and compare with the results obtained only during the loading phase, the root mean square (RMS) of the differences between systems was calculated for each silicone sample. The materials testing machine results for each load step was used as reference and the values from the motion analysis system subtracted from them, resulting in the absolute difference. The RMS used these values (one for each step) and yields a unique difference result, for both the whole cycle and for the loading phase only.

3.3. Results

Deformation

In all tests, the maximum vertical deformation acquired by the silicone samples did not exceeded 3 mm, and occurred when the maximum force of 575 N was applied. The results (Table 3.1) obtained on the materials testing machine were always higher than those from the motion analysis system. The deformation values provided by the equipment considered as the reference were between 37% and 64% higher, if a complete loading and unloading cycle is considered, and the percentage increases along with the silicone hardness. However, during the loading phase of the compression, the difference tends to be more constant and varies from 12% to 19%, as shown in Figure 3.7. The RMS from all loading/unloading cycle reached its maximum value on the hardest silicone (2% of acetone), 0.27 mm, and is slightly less when only the loading period is observed, as reported in Table 3.1.

TABLE 3.1 – Maximum vertical deformation measured on both MAS and MTM for each silicone sample; percentage of the difference between methods and the root mean square difference for the complete cycle and for only the loading phase.

Sample	MVD MAS (mm)	MVD MTM (mm)	Maximum difference - all cycle (%)	Maximum difference - loading (%)	RMS difference - all cycle (mm)	RMS difference - loading (mm)
Silicone 2%	1.83	2.16	63.8	18.9	0.27	0.25
Silicone 5%	1.98	2.24	38.2	11.8	0.19	0.17
Silicone 10%	2.41	2.71	37.0	13.6	0.22	0.19

MVD, maximum vertical deformation; MAS, motion analysis system; MTM, materials testing machine; RMS, root mean square.

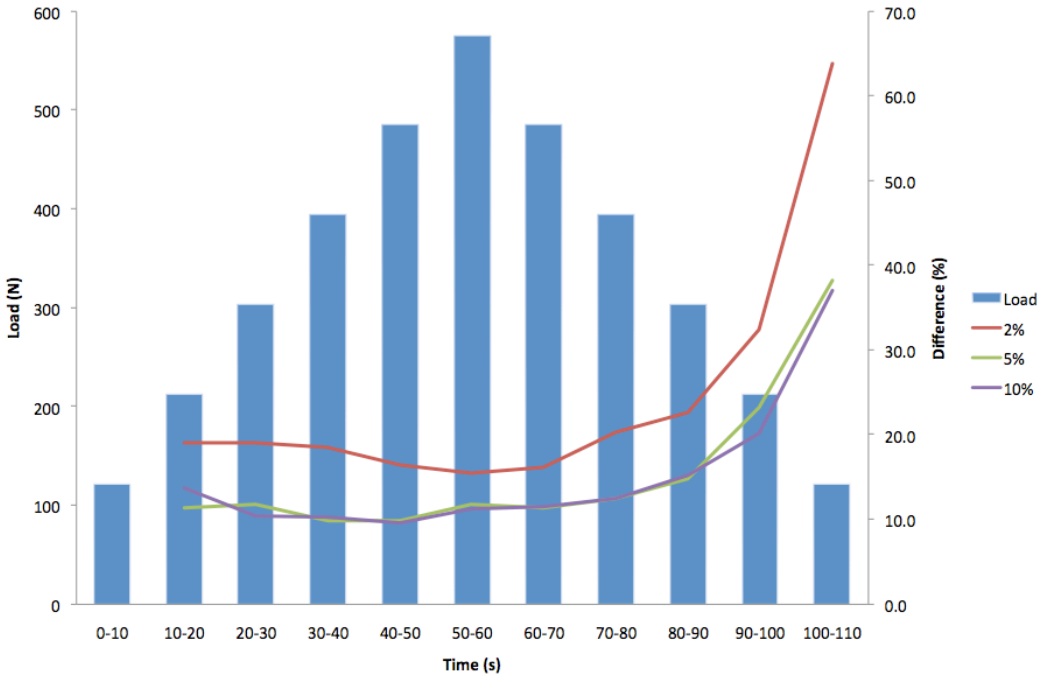

FIGURE 3.7 – Percentage of the difference between the vertical deformation of the silicone samples (2%, 5%, and 10% of acetone) measured on the motion analysis system and on the materials testing machine during a single cycle of loading and unloading.

Stiffness

The results for stiffness highlight the differences amongst the samples, clearly showing a harder silicone on the sample with 2% of acetone and a softer material when the amount of thinner was 10%. Considering the method, the stiffness calculated from the portion comprised between 30% and 85% of the loading cycle was greater on the tests taken at the motion analysis system for all samples. Using this equipment, the slope of the load-deformation curve at this section varies from 10% to 17% greater than the values obtained on the material testing machine, with the highest value found on the hardest silicone sample, as shown in Table 3.2. As an example, it is highlighted in Figure 3.8 the portion of the load-displacement curve used to estimate this property.

TABLE 3.2 – Stiffness measured on both MAS and MTM for each silicone sample, and the percentage of the difference between methods.

Sample	MAS (kN/m)	MTM (kN/m)	Difference (%)
Silicone 2%	262.5	225.2	16.5
Silicone 5%	232.5	211.9	9.7
Silicone 10%	190.2	171.9	10.7

MAS, motion analysis system; MTM, materials testing machine.

Energy Dissipation Ratio (EDR)

Load-deformation curves provide the necessary information to calculate the EDR, as the area between the loading and unloading curves, or hysteretic loop, relative to the total area of the loading curve. Figure 3.8 shows one of

these curves, obtained using the silicone sample with 5% of acetone on both methods.

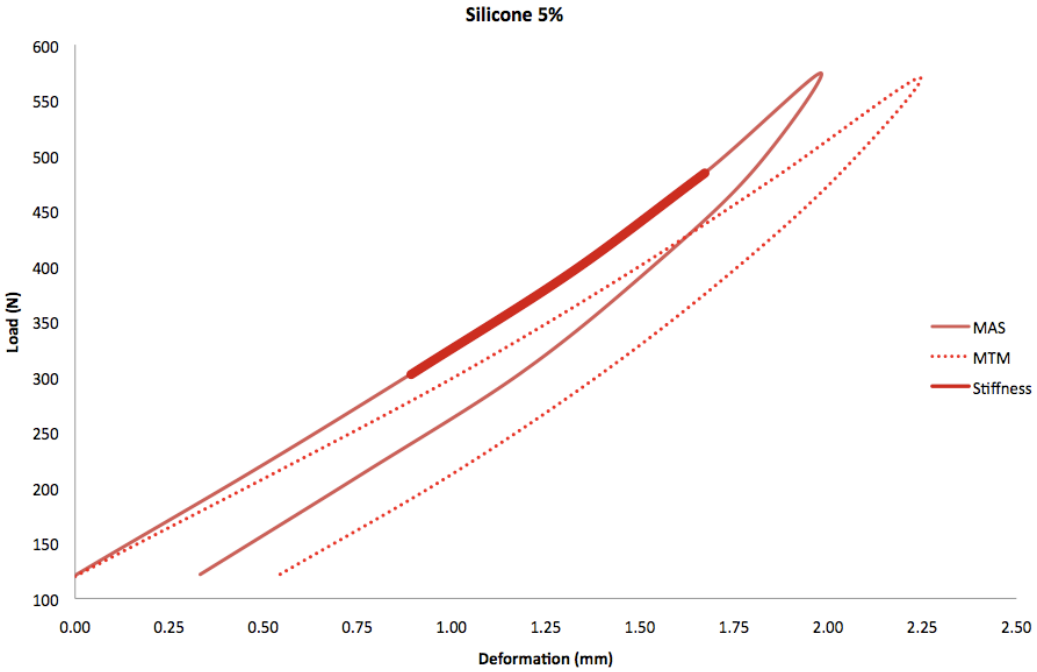

FIGURE 3.8 – Load-deformation curves form the silicone sample with 5% of acetone, measured on the motion analysis system (MAS) and on the materials testing machine (MTS) during a single cycle of loading and unloading. The portion of the MAS curve used to calculate the stiffness is highlighted.

The total energy absorbed during the compression cycle was less when measured in the motion analysis system compared to the results from the materials testing equipment, but higher on softer samples (5% and 10% of acetone) on both methods. The range of 13% to 21% calculated from the motion analysis results provides the largest percentage of difference with the other method, reaching 42% of deviation, as show in Table 3.3.

TABLE 3.3 – Energy dissipation ratio (EDR) measured on both MAS and MTM for each silicone sample, and the percentage of the difference between methods.

Sample	**MAS (%)**	**MTM (%)**	**Difference (%)**
Silicone 2%	12.8	21.9	41.6
Silicone 5%	21.1	27.7	23.8
Silicone 10%	19.0	24.3	21.8

MAS, motion analysis system; MTM, materials testing machine.

3.4. Discussion

Tests executed on three samples of a soft and elastic material indicate that motion analysis system can collect data from small deformations and yield results comparable to tests done on reference equipment. The RMS of the difference between the vertical deformation values from both systems suggests the systematic error found on the motion analysis system, however some considerations are necessary.

Due to the pilot nature of the present investigation, only a single loading/unloading test with each sample on both systems was performed, which clearly does not represent a comprehensive reliability test. The objective was to test the motion analysis system's capability of measuring small deformations, comparable to those obtained on the heel pad, and estimate the systematic error embedded into this information. Therefore, results obtained show trends and no statistical tests could be applied in order to verify data repeatability. For future research, it is recommended a consistent reliability test be performed in order to obtain more complete results.

The maximum absolute difference between the deformation results can reach 64% if the full loading/unloading cycle is considered. However, Figure 3.7 shows that this values increase considerably at the end of the unloading phase, and is more consistent during the loading period, when variation does not exceed 20%. This is caused by the non-linear characteristics of the material, as during the unloading phase some residual deformation is still present in the samples. The materials testing machine could detect a higher amount of this residual, defined as the difference of the deformation obtained with the same load value between the unloading and loading phases, as exemplified for the silicone with 2% of acetone in the Figure 3.9. It means that for a particular load, the materials testing machine identified more deformation residuals than the motion analysis system, and the same behavior was found for the two other samples. The use of the latter system

for collection of unloading deformation of soft materials can be therefore considered less accurate, and this fact also contributes to the high differences found on the EDR.

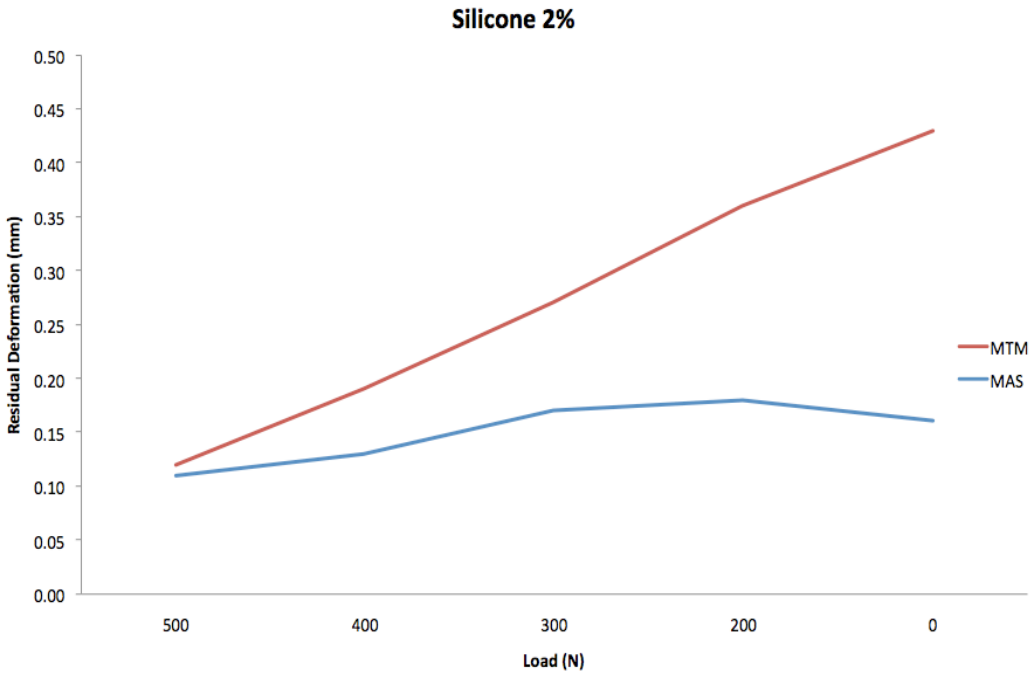

FIGURE 3.9 – Residual deformation during the unloading phase for the silicone with 2% of acetone, measured on the motion analysis system (MAS) and on the materials testing machine (MTS).

The RMS of the differences between deformations using both methods does not differ whether the entire cycle is considered or only the loading phase. Values shown in Table 3.1 reach a maximum of 0.27 mm for the complete cycle and 0.25 mm for the loading part. As a measure that takes into account all differences occurring throughout the period analyzed, it can be considered the associated systematic error of the measures. Therefore, the motion analysis system showed during this pilot investigation an underestimation of less than 0.3 mm of the measurements using 3 mm hemispherical markers. This systematic error is greater than the residual calibration error of 0.12 mm, and both have to be taken into account when measuring vertical deformations.

Due to the stepwise nature of the test, load-deformation curves were obtained using 11 single values, which can characterise the experiment as a quasistatic cycle. Therefore, stiffness data were based on the slope of a line composed by only 3 points (30% to 85% of the loading cycle), a simplification that might not represent the dynamic behavior of the material. The difference between 10% and 17% obtained in the results is probably consequence of this reduced amount of data. The lines used to calculate the slope of the curves are shown in Figure 3.10, which clearly demonstrates the increase in the stiffness according to the silicone hardness.

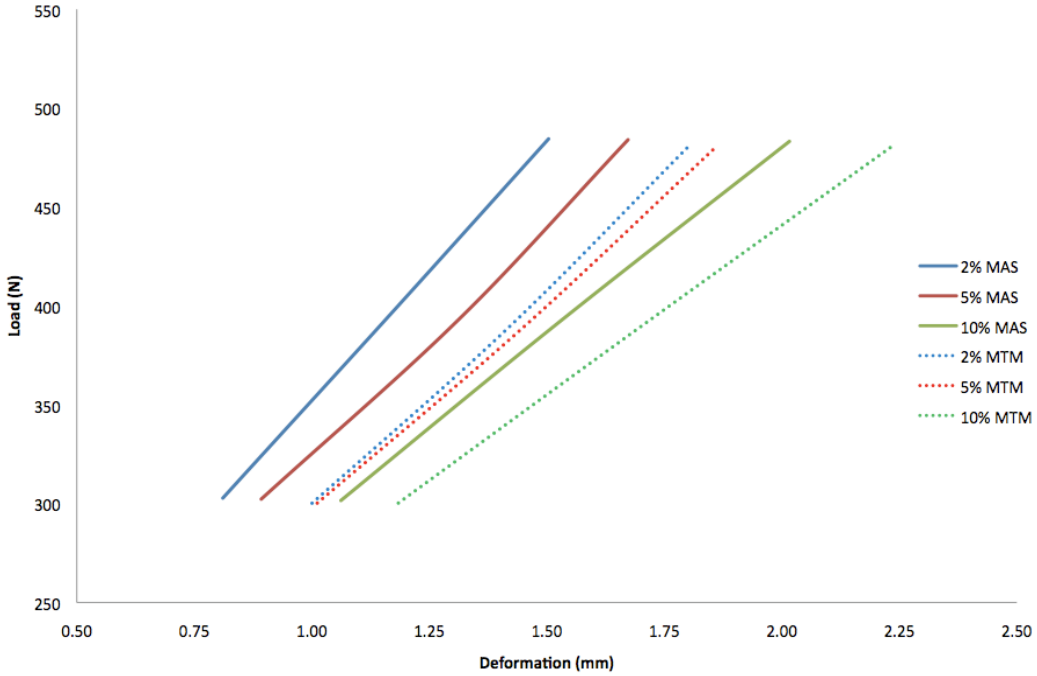

FIGURE 3.10 – Portion of the load-deformation curves used to calculate the stiffness of the silicone samples (2%, 5% and 10% of acetone). MAS, Motion Analysis System; MTM, Materials Testing Machine.

3.5. Conclusion

Values for deformation of a soft material measured with a motion analysis system are similar to those obtained with reference equipment, a materials testing machine, according to this pilot experiment. The RMS of the differences between equipments can be considered a trend for the systematic error found on the motion analysis system, corresponding to an underestimation of 0.3 mm on the vertical deformation. Results for stiffness were analogous, however the quasistatic nature of the experiment can be responsible to the differences of up to 17% observed. Energy dissipation ratios differed more than other variables, mainly because of the discrepancies found on unloading, when comparing the systems. Although this pilot study has identified the viability of the method, it is suggested that an investigation using a more rigorous repeatability method to accurately evaluate the errors associated with the motion analysis system when collecting small deformations would be needed before it was widely adopted as a technique.

4. Motion Analysis Testing

As seen previously, structural properties of the calcaneal heel pad have been estimated from measures made by techniques such as x-ray, ultrasound, impact tests or indentation, however all these methods report how the heel pad behaves only in the vertical direction. Under pressure, the heel soft tissue is indeed compressed vertically, but also expands medio-laterally and posteriorly, and those systems are not able to gather these dimensional changes. Motion analysis systems have the ability to capture 3D movements, opening a novel way to understand how the heel pad deforms in three-directions. Associated with force plate measures of loading, this new technique provides the necessary information to estimate structural properties of this tissue.

This chapter describes an experiment involving measurements of the heel pad deformation on healthy young adults during a dynamic loading and unloading task using motion analysis, and the estimation of some structural properties like thickness, stiffness and energy dissipation ratio. A comparison of these properties between genders is also carried out, followed by a discussion regarding the method, results and recommendations for further investigations.

4.1. Methods

This section describes how the present investigation was conducted, detailing subjects, equipments, procedure, and the approach given to data analysis and statistics. All the procedures used on this study were submitted to and approved by the Departmental Ethics Committee of the Department of Bioengineering at the University of Strathclyde.

4.1.1. Subjects

This study recruited 18 healthy adults (10 males and 8 females) from the general University population. All volunteers received verbal and written explanations regarding the investigation and provided informed written consent to participate. Biometric and demographic personal data were kept confidential and each participant received a special code to keep their data anonymous. This code was composed of the letter "S" and a sequential number, e.g. "S01"for the first volunteer, "S02" for the second, etc.

Inclusion criteria/ exclusion criteria

Participants between 18 and 60 years old were recruited. Subjects with diabetes, musculoskeletal injury of the foot and ankle, atrophy of the heel pad (as defined by Kinoshita et al., 1996), or aged over 60 years old were excluded from participating.

Data from two participants were not included on the study due to technical problems on the acquisition process. The force plate used on the experiment had to be reset before each data collection in order to maintain its zero level and eliminate any incidental drift, however the investigator did not execute this procedure with these participants, invalidating all data collected. Therefore, the study was carried out with 16 participants. The subjects excluded were both males, S01 and S08.

Sample size justification

Considering that no published work reporting deformation of the heel pad measured exclusively with optical stereometric systems, and assuming

normal distribution of the heel pad stiffness, this pilot study was conducted with a sample size that allows statistical analysis and helps selecting the most appropriate primary outcome measure (Lancaster et al., 2004).

The recruitment of 16 participants is based on average Compressibility Index (CI, the ratio between the heel pad thickness under loading conditions to the thickness under unloaded conditions) reported in the literature (Hsu et al., 1998). The proposed sample size will have 80% power to detect a 15% change in the compressibility index of the heel pad between genders at an alpha of 0.05.

4.1.2. Equipments

Ultrasound

Measurements of unloaded heel pad thickness were taken by the investigator with a Convex/Linear Ultrasonic Scanner (Model HS-2000, Honda Electronics Co. Ltd., Toyohashi, JP). The probe used was a 7.5 MHz linear array ultrasound transducer with 50 mm (Model HLS-475M, Honda Electronics Co. Ltd., Toyohashi, JP).

Motion Analysis

To track the position of skin-mounted 3 mm hemispherical auto-reflective markers, a six-camera optical stereometric system (Vicon 612, Oxford Metrics, Oxford, UK) sampling at 120 Hz was used. A capture volume 1.2 m long, 0.4 m high and 1.2 m wide was employed with a maximal residual error of 0.15 mm. The maximum distance from each camera to the volume centre was 0.9 m.

Force data were acquired with one 40 x 60 cm Kistler force platform with four 3-component force sensors (Model 9281C, Kistler Instruments Ltd., Winterthur, CH) connected to a PC via an eight channel Kistler type 9865B charge amplifier. Anteroposterior (X), medio-lateral (Y) and vertical (Z) forces were sampled at a rate of 3000 Hz.

Collected at different rates, position and force data are synchronized automatically by Vicon system using its internal clock, and are stored in a proprietary file format. When both data are exported to an ASCII file for post processing, force values are downsampled to reach the same sampling rate as the position data. Therefore, only the first frame on each group of 25

frames from force data was used. No filtering method was applied in order to evaluate the behavior of the raw data.

All procedures were taken at the Movement Analysis Laboratory at the Department of Bioengineering, University of Strathclyde, Glasgow, UK.

4.1.3. Procedures

Demographic and biometric data

Standard demographic and biometric data including gender and self reported age were recorded. Height and weight were recorded to the nearest 0.5 centimeter and decimal kilogram fraction using a stadiometer and clinical scales, respectively.

Unloaded thickness

It was arbitrarily chosen that all measures and procedures taken to evaluate the heel pad were done on subject's right foot.

Unloaded thickness of the heel pad was measured with real-time ultrasonography, with the subject positioned prone and the right ankle plantarflexed at approximately 45 degrees to his/her leg. Sagittal sonograms of the heel pad were acquired with the aid of coupling gel to ensure minimal pressure was applied to the heel pad. The investigator held the probe vertically relating to the sole of the foot and adjusted its position to allow good image quality. This real-time image was frozen and the measure taken. Figure 4.1a shows the foot and probe positions and Figure 4.1b a sample of an ultrasound image collected.

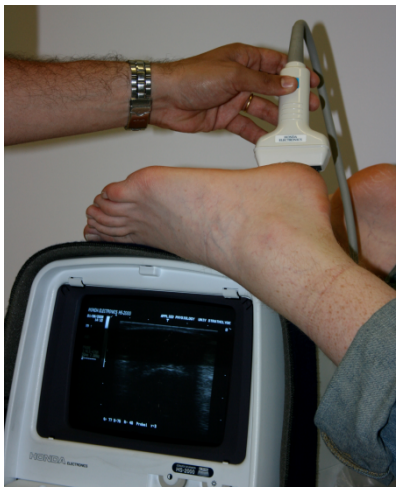

(a)

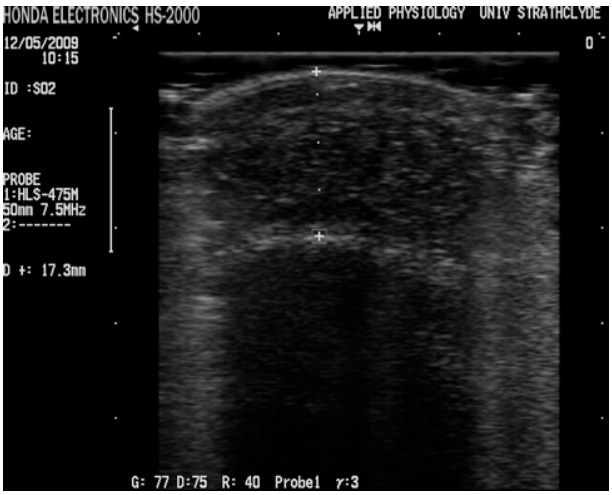

(b)

FIGURE 4.1 – (a) Measurement of the unloaded thickness of the heel pad using ultrasound. (b) Ultrasound image of the heel pad in the sagittal plane, the unloaded thickness is shown measured with the equipment caliper tool.

Dynamic test

Subjects were requested to stand barefoot on the floor to allow reflective markers being attached to the skin of the heel pad. The 3 mm hemispheric reflective markers were positioned on the subject's skin using hypoallergenic double-sided adhesive tape, cut and placed individually for each marker. A custom designed measurement template was used to ensure consistent marker placement on the skin surface. Subjects were asked to stand and distribute their weight on both feet equally, while the template was positioned, as shown in Figure 4.2a. Palpating the posterior aspect of the calcaneal tendon, the investigator marked with a pen a point at the middle of the tendon's width, and it was a reference to align the template midline. The markers positions were transferred to the skin using a pen (Figure 4.2b), followed by the placement of the double-sided adhesive tape (Figure 4.3a and Figure 4.3b), and eventually the reflective markers (Figure 4.3c).

(a) (b)

FIGURE 4.2 – (a) Subject's right foot and marker template. (b) A pen was used to transfer the marker points to the skin.

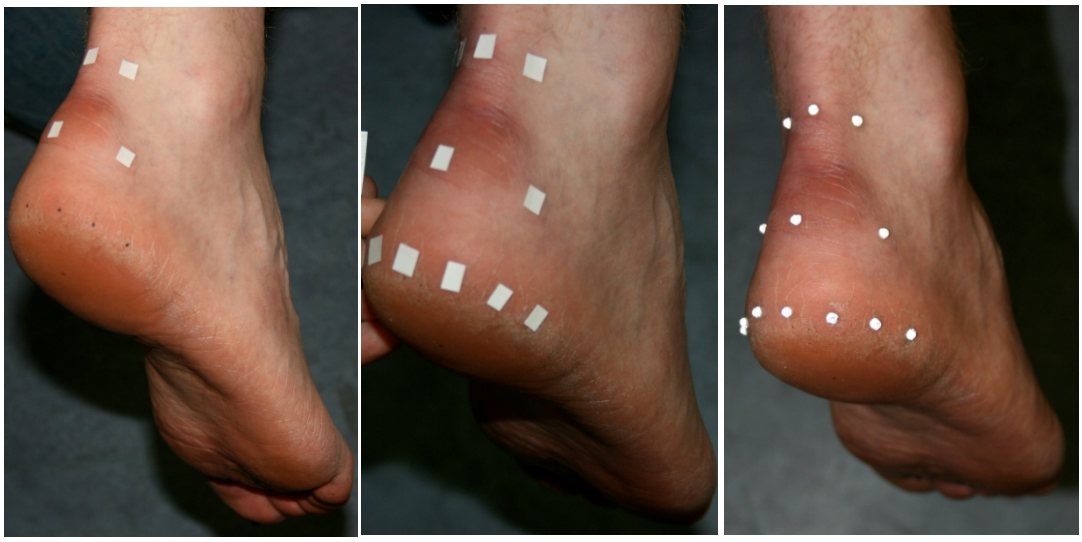

(a) (b) (c)

FIGURE 4.3 – (a) Subject's right foot during the marker placement procedure. The heel pad layer is marked with ink dots, the second and third layers are covered with double sided adhesive tape. (b) Foot with all three marker layers covered with double sided adhesive tape. (c) Right foot with all 13 marker set applied.

In total, 13 markers were attached on the foot, distributed in three different height or levels. Along the circumference of the heel pad seven markers were positioned 10 mm above the support surface, labeled as Heel Pad layer; a further three markers 40 mm above the support surface, called Level 1 layer. Level 2 was composed by three additional markers located at the lateral, medial and posterior aspects of the calcaneal tendon, at 80 mm above the ground level. Figure 4.4 highlights the markers and their labels.

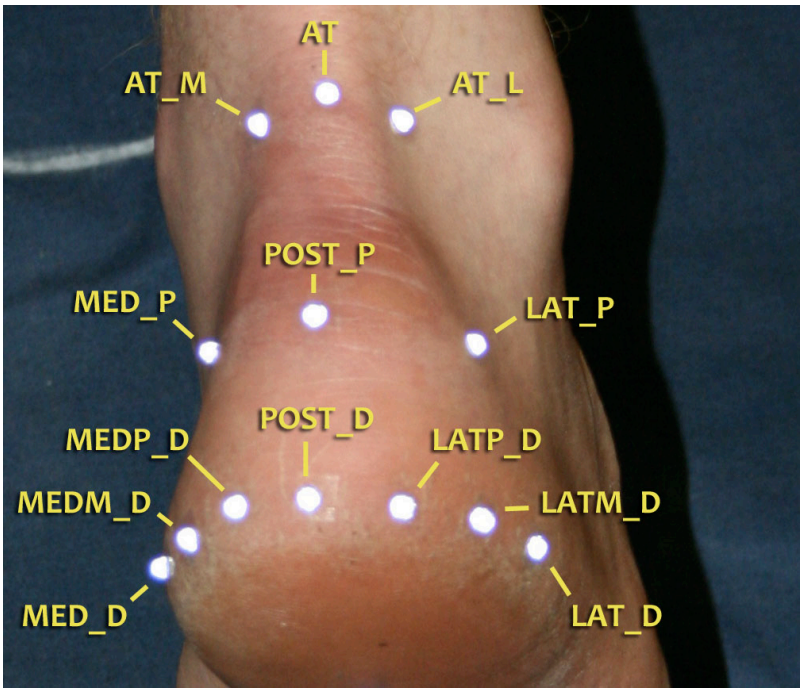

FIGURE 4.4 – Set of 13 reflective markers attached to the foot skin into three levels. At the most distal level is the Heel Pad layer, from medial to lateral: MED_D, MEDM_D, MEDP_D, POST_D, LATP_D, LATM_D, and LAT_D; at the intermediate level the Level 1 layer, from medial to lateral: MED_P, POST_P, and LAT_P; at the calcaneal tendon the Level 2 layer, from medial to lateral: AT_M, AT, and AT_L.

Once markers have been applied to the heel, the participant was guided to the force plate situated within the center of the laboratory. The subject was asked to stand on a wooden elevated platform (600 mm x 450 mm and 10 mm in height) positioned in front of the force plate, such that their right heel was free of the supporting wooden platform. At this position, only the participant's right rearfoot was free to contact the force plate with dorsiflexion of the ankle. The left foot was located slightly forward to the right, ensuring medial markers are within the field of view of the cameras. The floor under the capture volume was covered with a sheet to avoid any reflection to the cameras, and Figure 4.5 shows the setup.

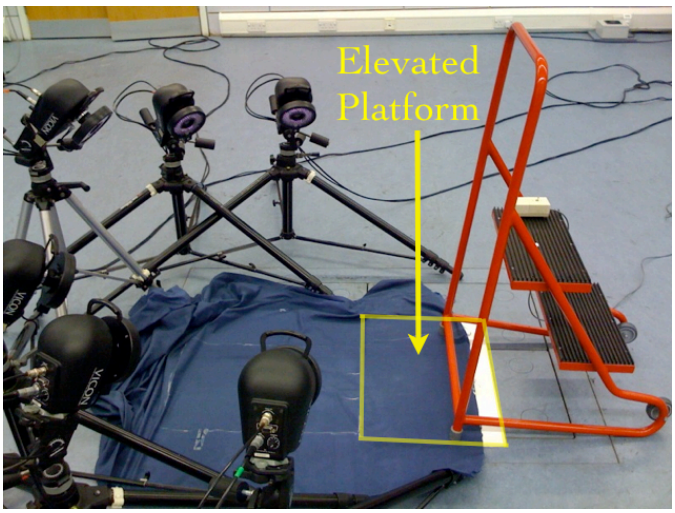

FIGURE 4.5 – Motion analysis setup. Six optic stereometric cameras positioned to capture the movement of 3 mm hemispherical reflective markers attached to subject's foot. A force plate, covered by a piece of sheet, captured loads. A wooden elevated platform allows the correct placement of subject's foot, ensuring that the rearfoot could be free to contact the force plate.

Subjects were asked to raise their right rearfoot and lower their heel on to the force plate, without removing their forefoot from the wooden platform, moving from full ankle plantarflexion to dorsiflexion. They were guided to load their body weight onto the right foot, smoothly, so as to produce as much compression as possible. To help stabilize the volunteer throughout the movement, a secure stair handle was provided for subjects to hold, as shown in Figure 4.6a and Figure 4.6b. Following an adequate familiarisation period, three trials were collected, with each trial consisting of five repetitions of the same loading-unloading movement, as detailed in Figure 4.7a and Figure 4.7b. A metronome, set at a rate of 1 Hz, helped control the loading and unloading frequency.

(a) (b)

FIGURE 4.6 – Data collection procedure. (a) Subject's right foot raised. (b) Subject compressing the heel pad against the force plate (covered by a piece of sheet). Loading and unloading data were captured at this time.

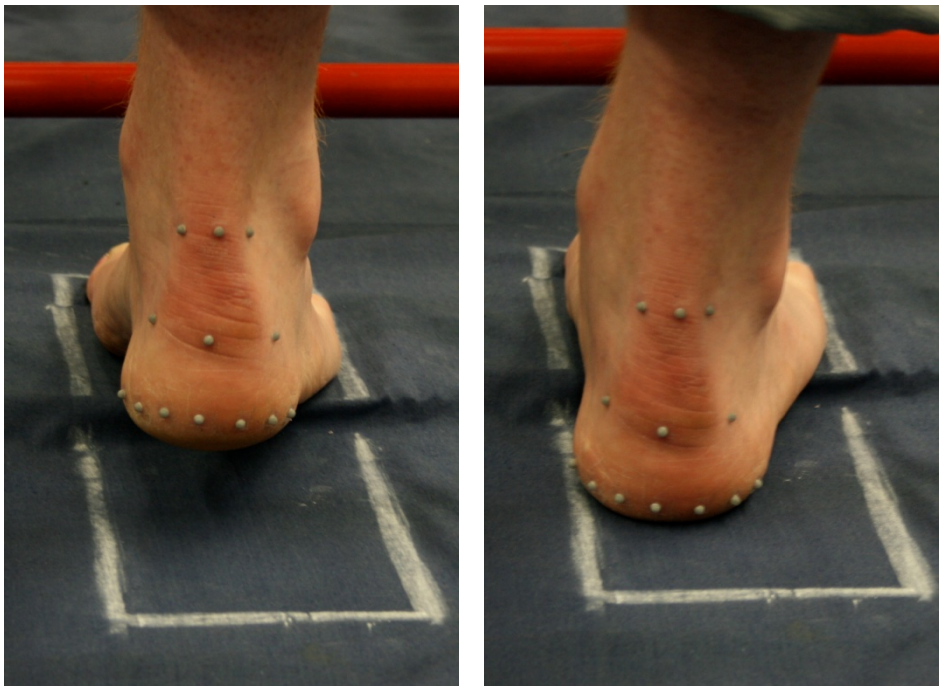

(a) (b)

FIGURE 4.7 – Details of the loading and unloading procedure. Subject's forefoot is positioned on the elevated platform, while the rearfoot is free to move up and down. The force plate is covered by a piece of sheet and collects the lodas applied by the heel. (a) Subject's right foot without any contact with the force plate. (b) Heel pad under compression.

4.1.4. Data analysis

Demographic and biometric data

Body mass index (BMI) was calculated for each participant, as a tool to compare the study population weight and height (Keys et al., 1972). It was carried out using the following equation:

$$BMI = \frac{\text{weight (kg)}}{(\text{height (m)})^2}$$

Equation 4.1 – Body mass index (BMI).

Unloaded thickness

An average of 3 consecutive ultrasound measurements was used on the analysis. The unloaded thickness was measured in the frozen image with the ultrasound caliper tool as the vertical distance between the inferior aspect of the medial calcaneus to the skin surface (Figure 4.1b).

Dynamic test

Each cycle of loading and unloading of the heel pad started at the first signal collected at the force plate and finished at the last, as diagrammatically shown in Figure 4.8. Therefore, only data obtained during contact time was used on the analysis, the foot movement upwards and downwards free of heel contact was discarded. The principle used was that once the skin surface touches the force plate, producing the initial signal, the heel pad would start its compression cycle. The displacement of the seven reflective markers layer,

attached to the pad itself, will match the displacement of the pad. Therefore, with cycles lasting approximately 1 Hz each, an average of 120 frames were collected, consisting of three position coordinates (x, y, and z) of each marker relative to the Laboratory coordinate system, and data from the force plate: forces and moments in three directions (x, y, and z). Only the vertical (z) component of the force was used in the analysis.

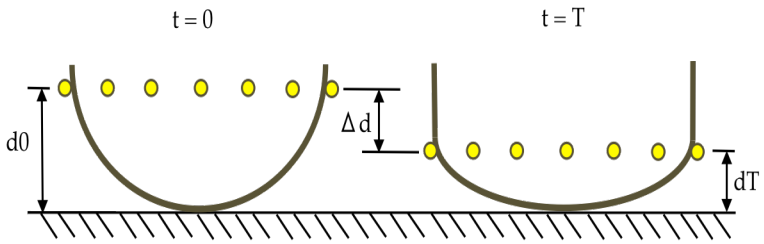

FIGURE 4.8 – Diagrammatic description of the dynamic test. At initial heel contact (time t=0) the distance between the markers and the force plate is d0. At any given time during heel compression (time t=T) this distance is dT. The heel deformation (Δd) is calculated as the difference between d0 and dT.

The principal structural properties (thickness, CI, stiffness and EDR) of the heel pad were calculated based on force and displacement data throughout the cycle. All data collected on the motion analysis system were exported to an ASCII format file and imported into spreadsheet software Microsoft Excel (Microsoft Corp., Washington, USA) for analysis.

To test whether the heel pad markers were moving upwards along with the skin, generating a relative movement between the inner tissue and the surrounding skin, the other two layers of markers, with three markers each, were used as a reference. Throughout each cycle, the vertical position of each marker was used to compare the relative distance between the markers at the Heel Pad level and marker Levels 1 and 2, in different locations. An average of the position of medial markers at the Medial Heel Pad Level (MED_D, MEDM_D, and MEDP_D) was calculated and the distance between this average and the medial marker located at Level 1 (MED_P) computed, as highlighted by the arrow D in Figure 4.9. This procedure was repeated for

each frame of the cycle, providing a dynamic map of the relative movement between the layers of markers. The same approach was given between an average of the posterior markers formed by MEDP_D, POST_D and LATP_D and the higher levels, and also the lateral markers, LATP_D, LATM_D, and LAT_D. Figure 4.9 illustrates the method used on this analysis.

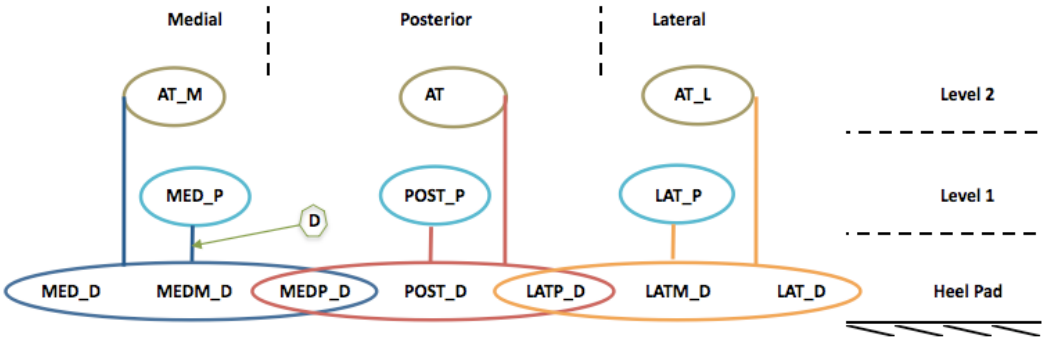

FIGURE 4.9 – Method used to calculate the relative movement between markers positioned at the Heel Pad level and Levels 1 and 2. Average of the vertical position of three groups of Heel Pad level markers was calculated (Medial Heel Pad Level: MED_D, MEDM_D, and MEDP_D; Posterior Heel Pad Level: MEDP_D, POST_D, and LATP_D; Lateral Heel Pad Level: LATP_D, LATM_D, and LAT_D) and the vertical distance between these values and medial, posterior, and lateral markers at Level 1 (MED_P, POST_P, and LAT_P) and Level 2 (AT_M, AT, and AT_L) used on the analysis. Arrow D illustrates the medial distance from Medial Heel Pad level to Level 1.

Using the force plate signal as the determinant of the beginning and end of each cycle, the frame prior the first positive signal at the force plate was selected as the initial, setting its time to zero (t=0). Subsequent frames provided information about loading and unloading, and the last positive value on the force plate indicated the final unloaded value, and this frame was selected as the final one.

Vertical displacements, z coordinates, of each of the seven Heel Pad level markers (MED_D, MEDM_D, MEDP_D, POST_D, LATP_D, LATM_D, and LAT_D) were then calculated as the difference between the vertical coordinate of the marker at any frame during the cycle and its vertical position when t=0, the very instant when the heel touches the force plate. This procedure was also carried out on the medio-lateral and posterior

directions (y and x coordinates, respectively). This approach provided the 3D movement of each marker from the beginning of heel pad compression until the end of the unloading process.

For the vertical analysis, an average of the displacement of all seven markers at each instant was calculated, providing a single value for each frame collected. Similar approach was given to the posterior displacement, however focusing the interest on the most posterior aspect of the heel, only the markers at this location were used on the average: MEDP_D, POST_D, and LATP_D. The contribution of the medial and lateral markers on the posterior displacement was detected to be minimum, being discarded from the average.

Medio-lateral displacements were calculated as an average of the distances between two groups of opposite markers. Absolute position at y direction from the most anterior group of markers MED_D and LAT_D, and from the intermediate group MEDM_D and LATM_D was used to compute the distance between these markers, as illustrated by Figure 4.10. An average of these two measurements was taken for the first frame and considered as the unloaded medio-lateral distance. The same process was carried out on all subsequent frames, and the final medio-lateral displacement for each frame computed as the difference between the distance at any frame and at the unloaded distance.

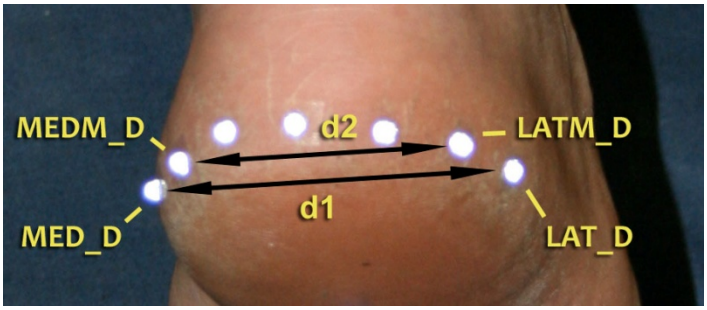

FIGURE 4.10 – Distances used to calculate the medio-lateral displacement of the heel pad, as an average of the distances between the markers MED_D-LAT_D (d1) and MEDM_D-LATM_D (d2).

Using these methods to compute vertical, medio-lateral and posterior displacements, in conjunction with loading and unloading values provided by the force plates, it was possible to derive other structural properties of the heel pad. However, due to the great amount of data from each participant, some data reduction must take place. The test protocol consisted on three sets of five repetitions each, totalising 15 cycles per participant. For each subject, a unique maximum deformation value on each direction was obtained by averaging all maximum deformation on each cycle; the same happened for the maximum peak vertical force during loading. However, load-deformation curves could not be averaged because each cycle contained a different number of frames, and no time normalisation was done.

The Compressibility Index (CI) (Jørgensen, 1985) was calculated as the ratio of the unloaded thickness (obtained via ultrasound) and the maximum deformation on the vertical direction, used as the loaded thickness, as follows:

$$\text{Compressibility Index (CI)} = \frac{(\text{unloaded thickness} - \text{max deformation})}{\text{unloaded thickness}}$$

Equation 4.2 – Data Used to Calculate the Compressibility Index (CI).

Stiffness is generally calculated as the slope of the load-deformation curve, however there is no agreement in the literature about the most representative portion of this curve to be used. de Clercq et al. (1994) used the initial third and final third to obtain two different stiffness values, while Aerts and de Clercq (1993) calculated it quite subjectively, defining it as the linear part of the curve. The value of the maximum load divided by the maximum deformation was also used (Hsu et al., 1998; Rome et al., 2001), however this approach does not take into account the transient aspect of the deformation.

The present study tried to contemplate the non-linear behaviour of the heel pad and assumed the stiffness as the slope of the linear regression line

between 30% and 85% of the loading portion of the load-deformation curve in the vertical direction. Therefore, each cycle yielded one stiffness value, and an average of all cycles was used for each participant on the analysis.

Load-displacement curves in the vertical direction were also used to calculate the energy dissipation ratio (EDR). The closed area between each upper loading curve and the lower unloading curve was computed by numerical integration based on the trapezoid rule, and denotes the dissipated energy. As defined in Equation 2.1, on Chapter 2, EDR is the ratio of the dissipated energy relative to the area under the loading curve. The areas were calculated using the software MATLAB (MathWorks Inc., Massachusetts, USA).

4.1.5. Statistical analysis

The dispersion of the vertical distance between markers located at Level 1 and Level 2 to markers at the Heel Pad Level during the entire cycle, calculated as the Coefficient of Variation (CV, ratio of the standard deviation to the mean distance), was used to evaluate whether any relative movement among levels exists.

All other statistical analysis used the Statistical Package for the Social Sciences (SPSS Inc., Illinois, USA). To evaluate normality of all variables, Shapiro-Wilk tests were carried out, and the distribution was normal on all variables but the medio-lateral displacement in women. Therefore, summary data was presented as means and standard deviations, and the differences in each of the normally distributed dependent variables were determined using independent t-tests. These variables are age, BMI, mean unloaded thickness, peak load, maximum vertical displacement, maximum posterior displacement, CI, mean stiffness, and mean EDR. Peak or maximum values represent the highest measured or calculated values among all cycles; mean results correspond to the average. The Compressibility Index was calculated using the maximum vertical displacement and mean unloaded thickness.

A non-parametric test (Mann-Whitney) was used to evaluate the difference in the medio-lateral displacement. To assess the correlation between variables, the Pearson's correlation test has been adopted. Significance at an alpha level of 0.05 was used for all tests.

4.2. Results

Demographic and biometric data

Table 4.1 shows demographic and biometric data from all participants and no statistically significant difference was found in terms of age, height, weight, and body mass index between males and females. At the date of data collection the average age was 29.9 (SD 5.4) (28.3 (SD 3.2) for males and slightly higher for females, 31.5 (SD 6.9)); the average height was 169 (SD 9) cm and weight was 68.9 (SD 9.0) kg (175 (SD 4) cm and 73.7 (SD 7.5) kg for males, and 162 (SD 7) cm and 64.1 (SD 8.1) kg for females, respectively). Body mass index was higher in females than males (24.3 (SD 3.4) and 23.8 (SD 1.9), respectively), and 24.1 (SD 2.7) when considering all participants.

TABLE 4.1 – Demographic (gender, age) and biometric (height, weight, and BMI) data from participants.

Subject	Gender	Age (years) *	Height (cm)	Weight (kg)	BMI (kg/m^2)
S02	Female	24.2	163	54.1	20.3
S03	Female	37.4	163	59.9	22.5
S04	Male	34.1	181	75.2	22.9
S05	Male	23.7	172	79.8	26.9
S06	Male	27.4	180	81.7	25.2
S07	Male	26.2	170	62.3	21.5
S09	Male	28.7	175	72.1	23.5
S10	Male	26.2	176	75.9	24.5
S11	Female	23.7	164	63.1	23.4
S12	Female	41.1	164	77.0	28.6
S13	Female	36.2	162	74.0	28.2
S14	Female	35.3	172	68.1	23.0
S15	Female	23.9	145	58.6	27.8
S16	Female	30.1	168	58.0	20.5
S17	Male	30.2	180	80.0	24.6
S18	Male	29.9	172	62.7	21.1

* age at date of data collection; BMI, body mass index.

Dynamic test

The maximum Coefficient of Variation (CV) of the distance between each of the three groups of heel pad level markers (Medial, Posterior and Lateral, as seen in Figure 4.9) and Level 1 and Level 2 markers was obtained for each cycle from each participant. The highest values from all subjects are shown in Table 4.2.

TABLE 4.2 – Highest Coefficient of Variability (CV) of the distances between Medial, Posterior, and Lateral Heel Pad Level markers and Level 1 and Level 2 markers.

Location	**Maximum CV (%)**
Medial Heel Pad Level to Level 1	3.64
Medial Heel Pad Level to Level 2	2.22
Posterior Heel Pad Level to Level 1	1.21
Posterior Heel Pad Level to Level 2	0.87
Lateral Heel Pad Level to Level 1	1.00
Lateral Heel Pad Level to Level 2	1.06

Detailed values for all measured and calculated structural properties evaluated on this study for each participant are displayed in Table 4.3, followed by respective mean and standard deviation. For young adults compressing the heel pad with an average load of approximately 400 N, the soft tissue experiences a vertical compression of 8 (SD 0.6) mm, and expands medio-laterally by 3.1 (SD 0.5) mm and posteriorly by 2.6 (SD 0.4) mm. The mean vertical compression corresponds to half the value of the unloaded pad thickness. During the loading phase, the mean stiffness is 212 kN/m, and the mean absorbed energy throughout the loading and unloading exercise is 22.3 %.

TABLE 4.3 – Peak Load, Mean Unloaded Thickness (UT), Maximum Vertical Displacement (VD), Maximum Medio-Lateral Displacement (MLD), Maximum Posterior Displacement (PD), Compressibility Index (CI), Mean Stiffness (S), and Mean Energy Dissipation Ratio (EDR) for all participants. The last row represents mean (standard deviation).

Subject	Sex	Peak Load (N)	UT (mm)	VD (mm)	MLD (mm)	PD (mm)	CI	S (kN/m)	EDR (%)
S04	M	521	19.3	8.4	2.3	2.9	0.56	367	14.8
S05	M	539	15.0	8.8	3.6	2.3	0.41	311	23.9
S06	M	520	14.3	8.2	3.5	2.7	0.42	315	16.7
S07	M	303	19.1	7.8	3.0	3.0	0.59	117	18.8
S09	M	328	19.6	7.1	3.6	2.9	0.64	193	26.0
S10	M	470	17.0	8.4	3.0	2.4	0.50	259	22.9
S17	M	418	16.5	8.2	2.1	2.7	0.50	233	25.5
S18	M	404	14.1	7.4	3.1	2.7	0.47	219	26.7
S02	F	251	17.2	7.2	3.4	2.5	0.58	168	20.7
S03	F	330	15.3	7.8	3.1	2.7	0.49	183	22.6
S11	F	327	16.1	7.3	3.0	2.5	0.55	243	35.5
S12	F	406	15.4	8.6	4.2	3.8	0.44	140	1.6
S13	F	400	15.3	7.6	2.8	2.3	0.50	218	32.3
S14	F	341	15.3	8.4	3.1	2.3	0.45	133	24.8
S15	F	385	19.4	9.0	2.8	2.6	0.53	116	11.4
S16	F	332	13.1	7.9	3.0	1.7	0.39	170	32.4
Mean (SD)		392 9 (84)	16.4 (2.1)	8.0 (0.6)	3.1 (0.5)	2.6 (0.4)	0.50 (0.07)	212 (74)	22.3 (8.4)

M, male; F, female.

Discrete analysis of all properties in males and females is shown in Table 4.4. Heel pad stiffness was 47% higher in males than females ($P<0.05$). Stiffness was strongly correlated with peak vertical force in males ($r=0.95$, $P<0.01$) but not in females ($r=-0.17$, $P>0.05$). The BMI (Table 4.2) in women has a strong correlation with the peak vertical force ($r=0.89$, $P<0.01$) but not in men ($r=0.65$, $P>0.05$). For both males and females the BMI does not show strong correlation with the stiffness ($r=0.53$ for men and $r=-0.16$ for women, $P>0.05$).

TABLE 4.4 – Heel pad properties (values and standard deviations) in males and females.

	Male	Female
n	8	8
Peak Load (N)	438 (90)	347 (50) *
Mean Unloaded Thickness (mm)	16.8 (2.3)	15.9 (1.8)
Maximum Vertical Displacement (mm)	8.1 (0.6)	8.0 (0.6)
Maximum Medio-Lateral Displacement (mm)	3.1 (0.5)	3.2 (0.4)
Maximum Posterior Displacement (mm)	2.7 (0.2)	2.6 (0.6)
Mean Compressibility Index	0.51 (0.08)	0.49 (0.06)
Mean Stiffness (kN/m)	252 (79)	172 (43) *
Mean Energy Dissipation Ratio (%)	21.9 (4.5)	22.6 (11.5)

* Significant difference between groups $P < 0.01$

Typical vertical, medio-lateral and posterior deformation of the heel pad during vertical loading and unloading is shown in Figure 4.11.

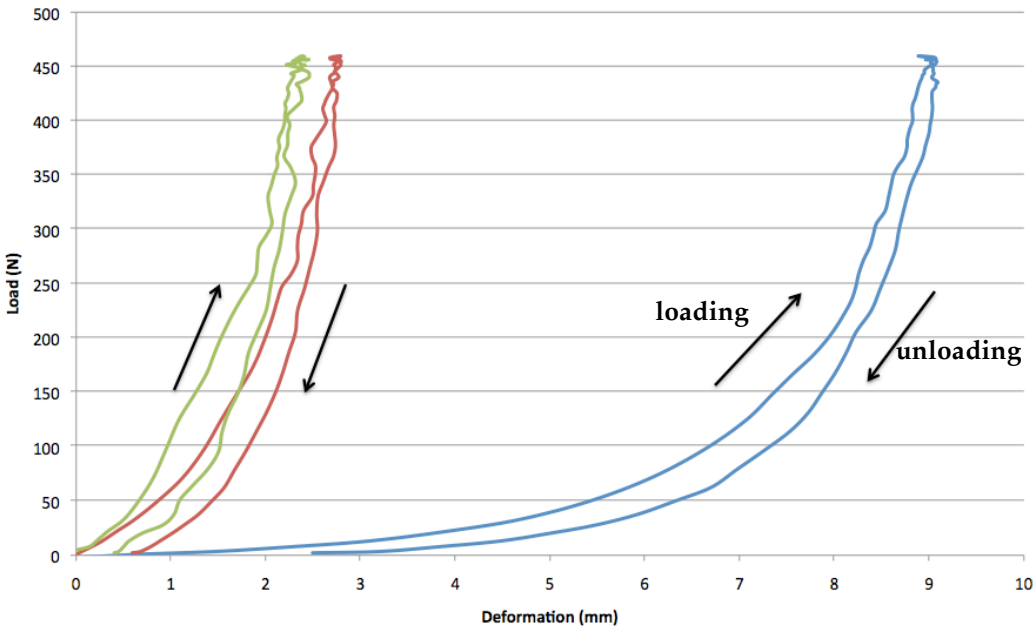

FIGURE 4.11 – Typical vertical (blue), medio-lateral (red) and posterior (green) deformation of the heel pad.

4.3. Discussion

The unloaded thickness of the heel pad in this study compared favorably to that reported using similar ultrasonic method in the literature, ranging from 12.4 mm to 19.8 mm (Rome et al., 1998b; Uzel et al., 2006a; Hsu et al., 2009). Comparable results were also observed with the vertical displacement of the soft tissue and the compressibility index, despite the method used to evaluate the compression and the peak load applied (Prichasuk et al., 1994; Uzel et al., 2006a; Tsai et al., 1999). Although the heel pad has been reported by several studies as thicker in men than in women (Prichasuk et al., 1994; Prichasuk, 1994; Turgut et al., 1999; Uzel et al., 2006a), the use of motion analysis technique did not evidence any significant differences between the genders on the three planes analyzed. Moreover, due to the innovative characteristic of this investigation, no report was found on the three-dimensional behaviour of the heel pad, therefore the results obtained for the medio-lateral and posterior displacements are, so far, unique.

Stiffness of the heel pad measured with the present method (212 kN/m), however, was higher than that found using impact tests (52 kN/m) (Aerts and de Clercq, 1993), or indentation tests (3.6 kN/m) (Hsu et al., 1998). On the other hand, it was lower then that obtained with cineradiography (634 kN/m) by de Clercq et al. (1994) or compared to *in vitro* tests using material testing machines, which range from 504 to 1160 kN/m, conduted by Aerts et al. (1996) and Bennett and Ker (1990).

The method chosen to evaluate stiffness, allied to the definition on how to calculate this property, are the main sources of discrepancies on the values obtained. Impact tests exert a high load on the tissue during a short period of time, whereas indentation uses a measuring probe that concentrates the applied pressure over a small area of the heel, and these methods do not simulate how the soft tissue is compressed during daily activities, such as standing or walking. *In vitro* investigations have the ability to accurately control the experiment, however the influence of the whole leg as part of the

shock absorbency system, as discussed by Aerts et al. (1995), is generally not evaluated. There is also no agreement on which portion of the load-displacement curve is most representative to describe stiffness. It is depicted from the vertical curve (blue) in Figure 4.11 that great majority of the deformation occurs at the initial compression stage, followed by a rapid change of the load, which is associated with a small increase in the deformation. The measured stiffness is a typical non-linear behaviour, which prevents a stiffness analysis be done simply by using the maximum load and deformation values. Calculated as the regression line between 30% and 85% of the loading and deformation curve, the results obtained in the present investigation tried to represent the most characteristic portion of the increase in stiffness during the compression period.

Despite methodological variances when comparing to other studies, this investigation found a significant difference in stiffness between male and females (Table 4.4). The lack of control over the amount of load applied by the subject when performing the exercise task did not seem to affect this outcome in males, as a strong correlation with the stiffness and the peak vertical force was found. A similar relation was not observed in females. There was a difference between the mean peak value between gender.

It is commonly accepted that increased thickness and decreased elasticity (which can lead to reduction of stiffness) are found in the population over 40 years old (Prichasuk et al., 1994; Ozdemir et al., 2004), probably due to several consequences of ageing, like degenerative alterations in the elastic adipose tissue, such as loss of collagen, and reduction of both elastin fibers and water content (Kinoshita et al., 1996). However, few studies have looked at gender differences. The male body composition is generally larger than female (Spitzer et al., 1999), which can lead to a larger fat content in adipose heel tissue chambers, and an increased internal pressure. As suggested by Ker (1999), this group of chambers that form the heel pad works as a sealed cushion to resists the externally applied loads. Consequently, the greater the content inside each chamber, the higher the resistance to deform. Men show an increased resistance to deform by the applied loads, although no

difference has been found neither on the unloaded thickness nor on the maximal deformation between genders.

The Energy Dissipation Ratio obtained was 22.3% when analyzing all subjects, and was comparable to studies using indentation method (23% to 71%) or *in vitro* investigations with material testing machines (28% to 48%), but smaller than impact tests (76%) or fluoroscopic measurements, which reported values of 69%. Similar to the stiffness analysis, methodological differences can restrict comparisons. Studies involving measurements under everyday activities, such as the fluoroscopic test when normal walking was performed (Wearing et al., 2009), tend to provide more reliable results. Therefore, the findings of the present study may be related to the loads applied and the rate of this loading, which are comparable to methods like indentation or materials testing machines. The peak loads executed by the participants are below those executed in normal walking, and the same happened to the loading and unloading rate. Kinoshita et al. (1996) demonstrated that there is a strong dependency of the energy storage capacity of the heel pad upon the rate of loading, corroborating the results.

The use of motion analysis system to evaluate deformities of the heel pad allied to force plate to collect the loads applied has demonstrated to be effective. The use of markers on different levels of the foot, to guarantee that only heel soft tissue movement was being collected, could be demonstrated by low values of the coefficient of variability of the distances between levels. The capture of the dynamic behaviour of the calcaneal soft tissue in three-dimensions can be extended to different populations, like older adults or children, and also to increase the understanding of different diseases, such as plantar heel pain or diabetes. However, some issues and difficulties found on the present study might help the development of future research.

A group of 7 reflective markers was used to collect 3D displacements of the heel soft tissue, as indicated in Figure 4.4. However, vertical, medio-lateral, and posterior maximum values were calculated based on averages of displacements from small sets of those markers. This approach was chosen to guarantee that occasional inability or difficulty of the motion analysis system

in capturing any marker during the loading and unloading exercise was balanced by the numerical average. Missing data is a result of the way the motion capture system reconstructs markers coordinates, and the parameters used to execute this task. In this study, some reconstruction parameters in the Vicon motion capture system were modified to allow the correct determination of the markers coordinates, and they are highlighted in Table 4.5.

TABLE 4.5 – Vicon reconstruction parameters.

Parameter	Value
Max Noise Factor	7.0
Intersection Limit (mm)	2.2
Residual Factor	0.53
Predictor Radius (mm)	3.0

Although these parameters could generate the coordinates to the majority of the data collected, some data were lost. Therefore, when a marker was not present in the data set at a particular moment, its coordinates were not present as well, and the use of an average with other markers eliminates this problem.

In future investigations, with the advent of systems with high-resolution cameras, the collection of data from small reflective markers tends to be less prone to errors like this. Therefore, the use of a set with fewer markers should simplify the subject preparation, data collection, and data analysis.

The most medial and lateral markers, MED_D and LAT_D (see Figure 4.4), and the posterior marker, POST_D, should not be removed because they represent the higher displacement in the medial-lateral and posterior directions, respectively. On the other hand, the two intermediate markers on each side (MEDM_D, MEDP_D, and LATM_D, LATP_D) can be replaced by a single marker medial and another single marker lateral, without any harm to the results.

Regarding the loading and unloading exercise, the data collection protocol does not restrict or control the amount of load exerted on the force

plate during the compression cycles. It limits the comparison between subjects, being clearly demonstrated by the poor correlation between peak load and stiffness in women. A different method to constrain this variable or normalize it, using a camera setup able to collect deformation during a normal gait for instance, should eliminate this restriction.

Another problem noticed only after the data collection had occurred was the force plate threshold, which is a minimum load value to be applied onto the force plate before it starts to provide useful reading. Any force exerted below this limit is discarded, it is a system preset, and during the experiment it was set to 9.8 N. Therefore, it is possible that some deformation might have been occurred before the first load signal arrive from the force plate. There is no workaround for data already collected with this setting, however assuming the results obtained are not dissimilar from those found on other studies, this problem was considered relevant, but not compromising.

Ultrasound images were used to measure the unloaded thickness of the heel pad, and the results obtained do not differ from those found in the literature. However, the method applied to collect these data could be improved to guarantee the same subject position on each measurement. Although the investigator have positioned subject's ankle dorsiflexed at approximately 45 degrees, both this angle and the angle from the sole of the foot to the ultrasound probe were not accurately the same on each measurement and among subjects. It is recommended therefore that a more precise tool, like a guidance rig, should be used to avoid this potential bias.

The pressure applied by the ultrasound probe to the sole of the foot in order to get the unloaded thickness is also a matter of discussion. The measurements were recorded to the nearest 0.1 mm, therefore inadequate pressure exerted on the probe could result in a reduced heel pad thickness. Although the investigator tried to minimize this problem by collecting data only when he noticed that no pressure was applied to the sole, a more reliable method should be chosen. The use of water as a coupling would make measurements more accurate, as being a medium where images can be taken without any physical contact between the probe and the heel pad.

Future investigations should evaluate the use of this method instead of the standard coupling gel.

4.4. Summary

The structural properties of the calcaneal fat pad can be estimated using a three-dimensional motion analysis system synchronized with a force platform. Preliminary findings show that the heel pad is compressed by 8.0 mm vertically, and expands 3.1 mm medio-laterally and 2.6 mm posteriorly. It was found that the vertical compression corresponds to half the value of the unloaded thickness, and the loading and unloading cycle absorbs 22.3% of the loading energy. The results suggest that males may have stiffer fat pads than females despite similar initial thickness.

5. Conclusion

Studies on the structural properties of the calcaneal fat pad have been undertaken with the ultimate objective of evaluating how changes in this structure can influence underlying diseases, or the opposite, whether the alterations are consequences of some conditions. In order to provide the necessary tools to compare healthy and non healthy subjects, it is necessary to have an understanding of how the heel pad behaves in terms of quantitative parameters in both situations. Therefore, many investigations have been conducted to report properties like unloaded and loaded thickness, Compressibility Index, stiffness, and energy dissipation ratio, among others.

However, there is still no agreement on what is the best equipment to collect data, and also on what kind of protocol can provide the most representative set of parameters. The present investigation tried to enrich this discussion introducing a novel approach in terms of measuring technique, proposing the evaluation of some structural properties of the heel pad using motion analysis systems synchronized with force plate data, using a pilot method to collect data from young healthy subjects.

The method was initially tested to verify its accuracy against reference equipment, where silicone phantoms were cyclically compressed and displacements in the order of magnitude of the vertical deformation of the heel pad were collected using both equipments. It was observed that motion analysis system tends to underestimate the displacements by 0.3 mm, which in a range of expected vertical displacements of 6 to 18 mm, is acceptable.

Results from human test show values similar to those reported by different investigators, however the use of a three-dimensional system allows the measurement of displacements in directions never reported so far. On the observation of a group of 16 healthy adults executing a series of exercises of loading and unloading their heel pads against a force platform,

the calcaneal fat pad deformed 8.0 mm vertically, 3.1 mm medio-laterally, and 2.6 mm posteriorly. The mean Compressibility Index was 0.50, indicating that the fat pad is compressed by its half unloaded thickness when loaded. The mean stiffness for all subjects was 212 kN/m, although there is no agreement on the literature regarding the most representative value, a significant difference was found between men and women, suggesting that males have a heel 47% stiffer than females. The energy dissipation ratio found for all participants was 22.3%, which corresponds to values found on studies using low loading values.

Summarising, the present study tested the use of motion analysis system and force plate data to collect small displacements. Accuracy was checked contrasting results of the compression of silicone calcaneal phantoms using motion analysis and a reference equipment. Test on young healthy volunteers provided substantial data from the human calcaneal fat pad, and structural properties were derived from values acquired using three-dimensional equipment, resulting in novel and constructive information on this field of knowledge.

References

Aerts, P., & de Clercq, D. (1993). Deformation characteristics of the heel region of the shod foot during a simulated heel strike: the effect of varying midsole hardness. *Journal of Sports Sciences* , 11 (5), 449-61.

Aerts, P., Ker, R., de Clercq, D., & Ilsley, D. (1996). The effects of isolation on the mechanics of the human heel pad. *Journal of Anatomy* , 188 (Pt 2), 417-23.

Aerts, P., Ker, R., de Clercq, D., Ilsley, D., & Alexander, R. (1995). The mechanical properties of the human heel pad: a paradox resolved. *Journal of Biomechanics* , 28 (11), 1299-308.

Alvarez-Nemegyei, J., & Canoso, J. (2006). Heel pain: diagnosis and treatment, step by step. *Cleveland Clinic Journal of Medicine* , 73 (5), 465-71.

Bennett, M., & Ker, R. (1990). The mechanical properties of the human subcalcaneal fat pad in compression. *Journal of Anatomy* , 171, 131-8.

Blechschmidt, E. (1982). The structure of the calcaneal padding. *Foot & Ankle* , 2 (5), 260-83.

Bohrer, S. P, & Ude, A. (1978). Heel Pad Thickness in Nigerians. *Skeletal Radiology , 3* (2), 108-112.

Buschmann, W., Hudgins, L., Kummer, F., Desai, P., & Jahss, M. (1993). Fatty acid composition of normal and atrophied heel fat pad. *Foot & Ankle* , 14 (7), 389-94.

Buschmann, W., Jahss, M., Kummer, F., Desai, P., Gee, R., & Ricci, J. (1995). Histology and histomorphometric analysis of the normal and atrophic heel fat pad. *Foot & Ankle International / American Orthopaedic Foot and Ankle Society [and] Swiss Foot and Ankle Society* , 16 (5), 254-8.

Cappozzo, A., Della Croce, U., Leardini, A., & Chiari, L. (2005). Human movement analysis using stereophotogrammetry. Part 1: theoretical background. *Gait & Posture , 21* (2), 186-96.

Cavanagh, P. (1999). Plantar soft tissue thickness during ground contact in walking. *Journal of Biomechanics* , 32 (6), 623-8.

Cavanagh, P., Morag, E., Boulton, A., Young, M., Deffner, K., & Pammer, S. (1997). The relationship of static foot structure to dynamic foot function. *Journal of Biomechanics* , 30 (3), 243-50.

Challis, J., Murdoch, C., & Winter, S. (2008). Mechanical properties of the human heel pad: a comparison between populations. *Journal of Applied Biomechanics* , 24, 377-381.

Chi, K.-J., & Schmitt, D. (2005). Mechanical energy and effective foot mass during impact loading of walking and running. *Journal of Biomechanics , 38* (7), 1387-95.

de Clercq, D., Aerts, P., & Kunnen, M. (1994). The mechanical characteristics of the human heel pad during foot strike in running: an in vivo cineradiographic study. *Journal of Biomechanics* , 27 (10), 1213-22.

Dykyl, D. (1999). Anatomy of the heel and rearfoot. In C. Ranawat & R. Positano (Eds.), *Disorders of the heel, rearfoot, and ankle* (pp. 1-17). New York: Churchill Livingstone.

Erdemir, A., Viveiros, M., Ulbrecht, J., & Cavanagh, P. (2006). An inverse finite-element model of heel-pad indentation. *Journal of Biomechanics* , 39 (7), 1279-86.

Gefen, A., Megido-Ravid, M., & Itzchak, Y. (2001). In vivo biomechanical behavior of the human heel pad during the stance phase of gait. *Journal of Biomechanics* , 34 (12), 1661-5.

Hsu, C.-C., Tsai, W.-C., Hsiao, T.-Y., Tseng, F.-Y., Shau, Y.-W., Wang, C.-L., et al. (2009). Diabetic effects on microchambers and macrochambers tissue properties in human heel pads. *Clinical Biomechanics (Bristol, Avon) , 24* (8), 682-6.

Hsu, C.-C., Tsai, W., Wang, C., Pao, S., & Shau, Y.-W. (2007). Microchambers and macrochambers in heel pads: are they functionally different? *Journal of Applied Physiology* , 102, 2227-2231.

Hsu, T.-C., Lee, Y.-S., & Shau, Y.-W. (2002). Biomechanics of the heel pad for type 2 diabetic patients. *Clinical Biomechanics (Bristol, Avon)* , 17 (4), 291-6.

Hsu, T.-C., Wang, C., Tsai, W., Kuo, J., & Tang, F. (1998). Comparison of the mechanical properties of the heel pad between young and elderly adults. *Archives of Physical Medicine and Rehabilitation* , 79 (9), 1101-4.

Hsu, T., Wang, C., Shau, Y., Tang, F., Li, K., & Chen, C. (2000). Altered heel-pad mechanical properties in patients with Type 2 diabetes mellitus. *Diabetic Medicine : a Journal of the British Diabetic Association , 17* (12), 854-9.

Irving, D., Cook, J., & Menz, H. (2006). Factors associated with chronic plantar heel pain: a systematic review. *Journal of Science and Medicine in Sport* , 9, 11-22.

Jahss, M., Kummer, F., & Michelson, J. (1992a). Investigations into the fat pads of the sole of the foot: heel pressure studies. *Foot & Ankle* , 13 (5), 227-32.

Jahss, M., Michelson, J., Desai, P., Kaye, R., Kummer, F., Buschman, W., et al. (1992b). Investigations into the fat pads of the sole of the foot: anatomy and histology. *Foot & Ankle* , 13 (5), 233-42.

Jørgensen U. (1985). Achillodynia and loss of heel pad shock absorbency. *The American Journal of Sports Medicine* , 13 (2), 128-32.

Kadaba, M., Ramakrishnan, H., & Wootten, M. (1990). Measurement of lower extremity kinematics during level walking. *Journal of Orthopaedic Research : Official Publication of the Orthopaedic Research Society , 8* (3), 383-92.

Kadaba, M., Ramakrishnan, H., Wootten, M., Gainey, J., Gorton, G., & Cochran, G. (1989). Repeatability of kinematic, kinetic, and electromyographic data in normal adult gait. *Journal of Orthopaedic Research : Official Publication of the Orthopaedic Research Society , 7* (6), 849-60.

Kanatli, U., Yetkin, H., Simsek, A., Besli, K., & Ozturk, A. (2001). The relationship of the heel pad compressibility and plantar pressure distribution. *Foot & Ankle International / American Orthopaedic Foot and Ankle Society [and] Swiss Foot and Ankle Society* , 22 (8), 662-5.

Ker, R. (1996). The time-dependent mechanical properties of the human heel pad in the context of locomotion. *The Journal of Experimental Biology* , 199 (Pt 7), 1501-8.

Ker, R. (1999). The design of soft collagenous load-bearing tissues. *The Journal of Experimental Biology , 202* (Pt 23), 3315-24.

Keys, A., Fidanza, F., Karvonen, M., Kimura, N., & Taylor, H. (1972). Indices of relative weight and obesity. *Journal of Chronic Diseases , 25* (6), 329-43.

Kinoshita, H., Francis, P., Murase, T., Kawai, S., & Ogawa, T. (1996). The mechanical properties of the heel pad in elderly adults. *European Journal of Applied Physiology and Occupational Physiology* , 73 (5), 404-9.

Lancaster, G., Dodd, S., & Williamson, P. (2004). Design and analysis of pilot studies: recommendations for good practice. *Journal of Evaluation in Clinical Practice , 10* (2), 307-12.

Ledoux, W., & Blevins, J. (2007). The compressive material properties of the plantar soft tissue. *Journal of Biomechanics* , 40 (13), 2975-81.

Ledoux, W., Meaney, D., & Hillstrom, H. (2004). A quasi-linear, viscoelastic, structural model of the plantar soft tissue with frequency-sensitive damping properties. *Journal of Biomechanical Engineering* , 126 (6), 831-7.

Lichniak, J. (1990). The heel in systemic disease. *Clinics in Podiatric Medicine and Surgery* , 7 (2), 225-241.

Ling, Choi, P.-C., Zheng, Y.-P., & Lau, K.-T. (2007). Extraction of mechanical properties of foot plantar tissues using ultrasound indentation associated with genetic algorithm. *Journal of Materials Science: Materials in Medicine* , 18 (8), 1579-86.

Martini, F.H. (2006). *Fundamentals of anatomy & physiology* (7th ed.). San Francisco: Benjamin Cummings.

McGinley, J., Baker, R., Wolfe, R., & Morris, M. (2009). The reliability of three-dimensional kinematic gait measurements: a systematic review. *Gait & Posture , 29* (3), 360-9.

Mickle, K., Steele, J., & Munro, B. (2008). Is the foot structure of preschool children moderated by gender? *Journal of Pediatric Orthopedics , 28* (5), 593-6.

Miller-Young, J., Duncan, N., & Baroud, G. (2002). Material properties of the human calcaneal fat pad in compression: experiment and theory. *Journal of Biomechanics* , 35 (12), 1523-31.

Ozdemir, H., Söyüncü, Y., Ozgörgen, M., & Dabak, K. (2004). Effects of changes in heel fat pad thickness and elasticity on heel pain. *Journal of the American Podiatric Medical Association , 94* (1), 47-52.

Pellicer, J., Garcia-Morales, V., & Hernandez, M. (2000). On the demonstration of the Young-Laplace equation in introdutory physics courses. *Physics Education , 35* (2), 126-129.

Prichasuk, S. (1994). The heel pad in plantar heel pain. *The Journal of Bone and Joint Surgery British Volume* , 76 (1), 140-2.

Prichasuk, S., Mulpruek, P., & Siriwongpairat, P. (1994). The heel-pad compressibility. *Clinical Orthopaedics and Related Research* , (300), 197-200.

Rome, K., Campbell, R., Flint, A., & Haslock, I. (1998a). Reliability of weight-bearing heel pad thickness measurements by ultrasound. *Clinical Biomechanics (Bristol, Avon)* , 13 (4-5), 374-375.

Rome, K., Campbell, R., Flint, A., & Haslock, I. (1998b). Ultrasonic heel pad thickness measurements: a preliminary study. *The British Journal of Radiology* , 71 (851), 1149-52.

Rome, K., Campbell, R., Flint, A., & Haslock, I. (2002). Heel pad thickness--a contributing factor associated with plantar heel pain in young adults. *Foot &*

Ankle International / American Orthopaedic Foot and Ankle Society [and] Swiss Foot and Ankle Society , 23 (2), 142-7.

Rome, K., & Webb, P. (2000). Development of a clinical instrument to measure heel pad indentation. *Clinical Biomechanics (Bristol, Avon)* , 15 (4), 298-300.

Rome, K., Webb, P., Unsworth, A., & Haslock, I. (2001). Heel pad stiffness in runners with plantar heel pain. *Clinical biomechanics (Bristol, Avon)* , 16 (10), 901-5.

Saltzman, C., Brandser, E., Berbaum, K., DeGnore, L., Holmes, J., Katcherian, D., Teasdall, R., Alexander, I. (1994). Reliability of standard foot radiographic measurements. *Foot Ankle International* , 15(12), 661-5.

Sammarco, G. J. (1988). Anatomy of the foot. In B. Helal & D. Wilson (Eds.), *The foot* (Vol. 1, pp. 31-65). Edinburgh: Churchill Livingstone.

Spears, I., & Miller-Young, J. (2006). The effect of heel-pad thickness and loading protocol on measured heel-pad stiffness and a standardized protocol for inter-subject comparability. *Clinical Biomechanics (Bristol, Avon) , 21* (2), 204-212.

Spears, I., Miller-Young, J., Sharma, J., Ker, R., & Smith, F. (2007). The potential influence of the heel counter on internal stress during static standing: a combined finite element and positional MRI investigation. *Journal of Biomechanics , 40* (12), 2774-80.

Spears, I., Miller-Young, J., Waters, M., & Rome, K. (2005). The effect of loading conditions on stress in the barefooted heel pad. *Medicine and Science in Sports and Exercise , 37* (6), 1030-6.

Spitzer, B., Henderson, K., & Zivian, M. (1999). Gender Differences in Population Versus Media Body Sizes: A Comparison over Four Decades. *Sex Roles , 40* (7/8), 545-565.

Tran, H., Charleux, F., Rachik, M., Ehrlacher, A., & Ho Ba Tho, M. (2007). In vivo characterization of the mechanical properties of human skin derived

from MRI and indentation techniques. *Computer Methods in Biomechanics and Biomedical Engineering , 10* (6), 401-7.

Tsai, W., Wang, C., Hsu, T.-C., Hsieh, F., & Tang, F. (1999). The mechanical properties of the heel pad in unilateral plantar heel pain syndrome. *Foot & Ankle International / American Orthopaedic Foot and Ankle Society [and] Swiss Foot and Ankle Society* , 20 (10), 663-8.

Turgut, A., Göktürk, E., Köse, N., Seber, S., Hazer, B., & Günal, I. (1999). The relationship of heel pad elasticity and plantar heel pain. *Clinical Orthopaedics and Related Research* , (360), 191-6.

Uzel, M., Cetinus, E., Bilgic, E., Ekerbicer, H., & Karaoguz, A. (2006a). Comparison of ultrasonography and radiography in assessment of the heel pad compressibility index of patients with plantar heel pain syndrome. Measurement of the fat pad in plantar heel pain syndrome. *Joint, Bone, Spine : Revue du Rhumatisme , 73* (2), 196-9.

Uzel, M., Cetinus, E., Ekerbicer, H., & Karaoguz, A. (2006b). Heel pad thickness and athletic activity in healthy young adults: a sonographic study. *Journal of Clinical Ultrasound : JCU , 34* (5), 231-6.

Wearing, S., Smeathers, J., Yates, B., Urry, S., & Dubois, P. (2009). Bulk compressive properties of the heel fat pad during walking: A pilot investigation in plantar heel pain. *Clinical Biomechanics (Bristol, Avon)* , 24 (4), 397-402.

Wong, W., Wong, M., & Lo, K. (2007). Clinical applications of sensors for human posture and movement analysis: A review. *Prosthetics and Orthotics International , 31* (1), 62-75.

Wrbaskić, N., & Dowling, J. (2007). An investigation into the deformable characteristics of the human foot using fluoroscopic imaging. *Clinical Biomechanics (Bristol, Avon)* , 22 (2), 230-8.

Yavuzer, G., Oken, O., Elhan, A., & Stam, H. (2008). Repeatability of lower limb three-dimensional kinematics in patients with stroke. *Gait & Posture , 27* (1), 31-5.